



Canopy bidirectional reflectance calculation based on Adding method and SAIL formalism: AddingS/AddingSD

Abdelaziz Kallel^{a,*}, Wout Verhoef^b, Sylvie Le Hégarat-Masclé^c, Catherine Ottlé^d, Laurence Hubert-Moy^e

^a CETP/IPSL, 10, 12 avenue de l'Europe 78140, Vélizy, France

^b National Aerospace Laboratory NLR, 8300 AD Emmeloord, The Netherlands

^c IEF/AXIS, Université de Paris-Sud 91405, Orsay Cedex, France

^d LSCE/IPSL, Centre d'Etudes de Saclay, Orme des Merisiers 91191, Gif-sur-Yvette, France

^e COSTEL UMR CNRS 6554 LETG/IFR 90 CAREN, Université de Rennes 2 Place du recteur Henri Le Moal 35 043, Rennes Cedex, France

ARTICLE INFO

Article history:

Received 1 June 2007

Received in revised form 19 May 2008

Accepted 24 May 2008

Keywords:

Radiative transfer theory

BRDF

Vegetation

Adding method

SAIL model

Kuusk' model

ABSTRACT

The SAIL model (proposed by Verhoef) is largely used in the remote sensing community to calculate the canopy Bidirectional Reflectance Distribution Function. The simulation results appear acceptable compared to observations especially for not very dense planophile vegetation. However, for erectophile dense crops (e.g. corn) the simulations appear less accurate. This inadequacy is due to the assumption that the multiple scattered fluxes are isotropically distributed. The SAIL parameters are interpretable at the level of elementary layer components. Now, the Adding method (initially proposed by Van de Hulst) provides a good framework to model the radiative transfer inside a vegetation layer, but its parameter estimation lies on very simple geometric modeling of the canopy. In this paper, we first propose an adaptation of the Adding method using the SAIL model canopy representation in the turbid case: it is called AddingS model. Such an approach allows to overcome the isotropy assumption. Second, AddingS is extended to the Discrete case: defining the AddingSD model. It allows to take into account the multi hot spot effect. Moreover, the AddingS and AddingSD models allow to check the energy conservation in respectively turbid and discrete cases. Finally, in order to keep reasonable time performance, a fast computation method was developed.

© 2008 Elsevier Inc. All rights reserved.

1. Introduction

Optical radiative transfer (RT) modeling (in terrestrial environments) aims at formulating the relationships between remote sensing measurements and the biophysical and biochemical features of the media. The Bidirectional Reflectance Distribution Function (BRDF) may be estimated using radiative transfer models which describe the interactions between the electromagnetic waves and the soil-vegetation system, i.e. the radiative fluxes inside the vegetation. These models allow the understanding of the observations acquired in various acquisition configurations (multi-date, multi-sensors, multi-channels, etc) by predicting BRDF values.

Radiative transfer theory was first proposed by Chandrasekhar (1950) to model radiation scattering in conventional media (rotationally invariant). This theory deals with radiation scattering in a given medium by modeling it as a set of parallel layers, diffusing and absorbing the solar flux. Being extended to non-rotationally invariant medium (typically foliage), numerous radiative transfer models have

been proposed for computation of canopy BRDF (Allen et al., 1970; Suits, 1972; Cooper et al., 1982; Verhoef, 1984, 1985; Verstraete et al., 1990a; Kuusk, 1994, 1995b). Recently, the inverse modeling was investigated (Verstraete et al., 1990b; Kuusk, 1991a, 1995a; Fanga et al., 2003; Combal et al., 2002). The SAIL model (Verhoef, 1984) is among the most widely used in case of crops canopies. Some improvements of SAIL model parameters have then been proposed (Verhoef, 1998) in order to take into account the hot spot effect (Kuusk, 1985, 1991b) and leaf specular reflectance. The SAIL model allows to derive a non-isotropic BRDF considering two diffuse fluxes (upward/downward flux) to model the multiple scattering of the radiant flux by the vegetation elements. These fluxes are added to the direct source flux and used to derive a directional radiance in the direction of the observation. In the SAIL model, the multiple scattered fluxes are assumed to be semi-isotropic, which is only an approximation. For example, vertical leaves do not emit radiation in vertical direction. Also, the SAIL model does not allow to take into account the multi hot spot effect (hot spot between multiple scattered fluxes). The SAIL parameters are interpretable at the level of thin layer (differential equations) and the whole vegetation scattering terms are derived by integration.

Besides, in the Adding method (Van de Hulst, 1981; Cooper et al., 1982; Lenoble, 1985), optical characteristics of canopy layers such as

* Corresponding author.

E-mail address: abdelaziz.kallel@cetp.ipsl.fr (A. Kallel).

reflectance and transmittance are directly defined and handled at the scale of the vegetation layer (as operators). Their physical interpretation is hence easier. However, the vegetation description is rather simplistic and the canopy internal geometry is represented with low accuracy. Indeed, in order to retrieve the adding operators for each layer, Cooper et al. (1982), like Smith et al. (1981), supposed that all layer elements are located in the middle of medium and that they were Lambertian surfaces. Therefore, the scattered flux of the whole layer is the sum of the fluxes scattered by every element weighted by the corresponding effective element surface (i.e. equal to its area after orthogonal projection on flux directions). This approximation does not take into account the interaction between layer elements. If the transmittance and the reflectance of the elements cannot be neglected, the contribution of the flux scattered by an element reaching another element to the flux scattered by this second element can be significant. For dense canopy layers, at near-infrared wavelength where leaf hemispherical reflectance (ρ) and transmittance (τ) values are between 0.45 and 0.55 (Jacquemoud & Baret, 1990), the interactions between layer elements should be taken into account. In order to adapt the Adding method to such a configuration, we need a more accurate estimation of the Adding scattering parameters. Since the Adding method operators are derived from the bidirectional reflectance and transmittance of the considered layer, in this study we propose to introduce the SAIL canopy description into the Adding formulation. The developed model in the turbid medium case is called AddingS. Such an evolution of the Adding method has important consequences for canopy BRDF estimation, especially by avoiding the assumption of the isotropy of diffuse fluxes assumed by SAIL. In the discrete case the correlation between light paths before and after scattering by some medium component should be taken into account. This phenomenon is the well-known hot spot effect. Based on the Kuusk model (Kuusk, 1985, 1991b), we propose the adaptation of AddingS to the Discrete case. The extended model is called AddingSD. This model allows both to conserve the energy and to take into account the hot spot effect between diffuse fluxes.

In the following, we first present the physical basis of our approach coupling SAIL and Adding in both the turbid and the discrete case. Secondly, we despite our model implementation: operator derivation and discretization. Finally, to validate our approach, some results are presented concerning the model symmetry, energy balance, and comparison with SAIL and then with 3-D models (RAMI II database).

2. Coupled Adding/SAIL modeling

The Adding method is based on the assumption that a vegetation layer receiving a radiation flux from bottom or top, partially absorbs it and partially scatters it upward or downward, independently of the other layers (Van de Hulst, 1981; Cooper et al., 1982; Lenoble, 1985). Thus, the relationships between fluxes are given by operators which allow the calculation of the output flux density distribution as a function of the input flux density distribution. As the Adding method vegetation layer operators depend on the bidirectional reflectance and transmittance, we propose to derive them both in the turbid and the discrete case based on respectively SAIL¹ and the Kuusk definition of the Hot Spot.

In this section, we first present the Adding operator definition, and secondly the derivation of the bidirectional reflectance and transmittance of a vegetation layer in both turbid and discrete cases corresponding respectively to the operators of the models AddingS and AddingSD.

¹ In this paper, we divide the SAIL BRDF terms by π , because these terms are multiplied by π in the original SAIL model [SAIL estimates E_o which is πL_o , where L_o is the radiance in the observation direction, see (Verhoef, 1984).

2.1. Adding operators reformulation in the continuous case

In this paragraph, we present a generalization of the Adding operators presented in Cooper et al. (1982) in the continuous case, dealing with radiance hemispherical distribution.

Fig. 1 shows the radiance L_e in the observation solid angle $\Omega_e = (\theta_e, \varphi_e)$ (θ_e is the zenithal angle and φ_e the azimuthal angle in the observation direction) provided by scattering of an incident source flux by the medium, $dE_i(\Omega_i)$, within a cone of solid angle $d\Omega_i = \sin(\theta_i)d\theta_i d\varphi_i$ (θ_i and φ_i are the zenithal and the azimuthal angles in the source direction). So the bidirectional reflectance is defined as follows:

$$r(\Omega_i \rightarrow \Omega_e) = \frac{dL_e(\Omega_i, \Omega_e)}{dE_i(\Omega_e)} = \frac{dL_e(\Omega_i, \Omega_e)}{L_i(\Omega_i) \cos(\theta_i) d\Omega_i},$$

where L_i is the radiance provided by the source.

Moreover, as illustrated in Fig. 1 by passing through the medium, the source radiation flux produces a radiance in the $\Omega_{e'}$ direction. So, like in the case of reflectance, the bidirectional transmittance can be defined as:

$$t(\Omega_i \rightarrow \Omega_{e'}) = \frac{dL_e(\Omega_i, \Omega_{e'})}{dE_i(\Omega_i)}.$$

For both cases, L_e is obtained by integrating the source flux over the hemisphere:

$$L_e(\Omega_e) = \underbrace{\int_{\Pi}}_{\text{over hemisphere}} \{t, r\}(\Omega_i \rightarrow \Omega_e) L_i(\Omega_i) \cos(\theta_i) d\Omega_i.$$

So, we define the two scattering operators \mathcal{R} and \mathcal{T} , that give the outward radiance L_e from an incident radiance defined over the whole hemisphere L_i :

$$\mathcal{R}[L_i](\cdot) = \int_{\Pi} r(\Omega_i \rightarrow \cdot) L_i(\Omega_i) \cos(\theta_i) d\Omega_i, \tag{1}$$

$$\mathcal{T}[L_i](\cdot) = \int_{\Pi} t(\Omega_i \rightarrow \cdot) L_i(\Omega_i) \cos(\theta_i) d\Omega_i. \tag{2}$$

From Eqs. (1) and (2), to derive the layer operators we should estimate the bidirectional reflectance and transmittance.

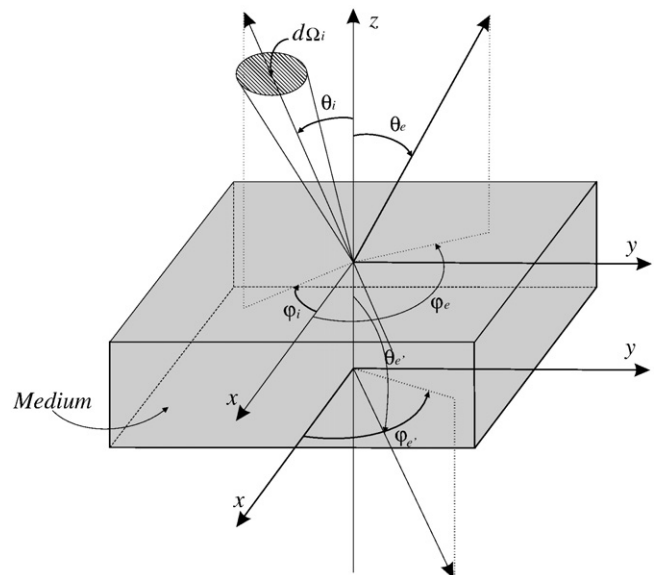


Fig. 1. Reaching a medium, the source radiation flux $dE_i(\Omega_i)$ provided from direction (θ_i, φ_i) within a solid angle $d\Omega_i$, produces a radiance at the top and at the bottom of canopy: respectively in direction (θ_e, φ_e) and $(\theta_{e'}, \varphi_{e'})$.

2.2. Turbid case: AddingS

For one vegetation layer, we present a derivation method of the top and the bottom bidirectional reflectances and the downward and the upward bidirectional transmittances which are called respectively, r_t , r_b , t_d and t_u . These bidirectional scattering terms are used to define the operators of the model AddingS. Note that, due to null size of components in the turbid case, there is no correlation between flux paths, and therefore there is no hot spot effect.

The SAIL model allows the calculation of the bidirectional reflectance of each vegetation layer: $r_t = \frac{\rho_{so}}{\pi}$. Assuming that the vegetation layer is formed by small and flat leaves with uniform azimuthal distribution, the layer has the same response when observed from the top or the bottom. Thus $r_b = r_t$ and $t_u = t_d$. So, only the derivation of t_d is presented here.

Depending on the physical phenomena inducing them, two kinds of transmittances can be differentiated: those provided from the extinction of the incident flux while passing through the layer, and those provided by the scattering of the incident flux by the vegetation components while reaching them. We called them respectively $t_{.s}$ and $t_{.d}$, where \times equals d (downward) or u (upward).

Assuming a vegetation layer located between altitude -1 and 0 and receiving only a direct flux $E_s(0)$ in direction $\Omega_s = (\theta_s, \varphi_s)$ from the top, by downward transmittance, a radiance $L_d(-1)$ exiting the layer in direction $\Omega_d = (\theta_d, \varphi_d)$ is produced at the bottom of layer (without taking into account the flux ‘reflected’ by the layers located below the considered one). L_d is divided into two radiances $L_{d,s}(-1)$ and $L_{d,d}(-1)$ created respectively by extinction and scattering. So, the downward transmittances are given by:

$$t_{d,s} = \frac{L_{d,s}(-1)}{E_s(0)}, \tag{3}$$

$$t_{d,d} = \frac{L_{d,d}(-1)}{E_s(0)}. \tag{4}$$

Note that for notation simplicity, the dependencies of $t_{d,s}$ and $t_{d,d}$ on the input and output angles are omitted.

In order to derive the expression of $t_{d,s}$, we first show the relationship between a direct flux E_s and its associated radiance L_s . Let us assume that a horizontal surface ds receives a radiation from a source located far enough in direction $\Omega_s = (\theta_s, \varphi_s)$, we can assume that it receives a directional flux $d\Phi$ with orientation angle Ω_s , i.e. $L_s(\Omega) = L_s(\Omega_s)\delta(\theta = \theta_s)\delta(\varphi = \varphi_s)$. Now, the flux $d\Phi$ received by the surface ds equals on the one hand $d\Phi = dsE_s$ and on the other hand $d\Phi = ds \int_{\Omega} L_s(\Omega) \cos(\theta) d\Omega$, therefore:

$$L_s = \frac{E_s \delta(\theta = \theta_s) \delta(\varphi = \varphi_s)}{\cos(\theta_s) \sin(\theta_s)}. \tag{5}$$

Passing through vegetation, E_s is extinguished by the vegetation, the relationship between $E_s(-1)$ and $E_s(0)$ is given by SAIL (Verhoef, 1985):

$$E_s(-1) = \tau_{ss} E_s(0). \tag{6}$$

Combining Eqs. (3), (6) and (5):

$$t_{d,s} = \frac{\tau_{ss} \delta(\theta = \theta_s) \delta(\varphi = \varphi_s)}{\cos(\theta_s) \sin(\theta_s)}. \tag{7}$$

Now, we propose to derive $t_{d,d}$. Like in the case of the radiance in direction of observation E_o calculation in the SAIL model (Verhoef, 1985), we can estimate $L_{d,d}$ using the fluxes E_s , E_- and E_+ : in sublayer at level z and thickness dz ,

$$L_{d,d}(z-dz) = L_{d,d}(z) + dz [w_d E_s(z) + v_d E_-(z) + v'_d E_+(z) - K_d L_{d,d}(z)], \tag{8}$$

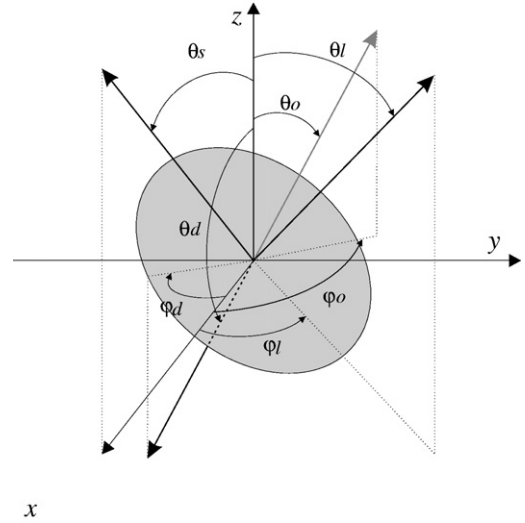


Fig. 2. Analogy between upward and downward radiances, given the directions of the source ($\theta_s, \varphi_s=0$), the leaf (θ_l, φ_l), the downward observation $\theta_d > \frac{\pi}{2}, \varphi_d$ and the upward observation ($\theta_o = \pi - \theta_d, \varphi_o = \pi + \varphi_d$). Reaching a leaf, the flux provides radiances on the observation directions either by reflectance or transmittance.

where w_d, v_d and v'_d are the scattering parameters, K_d is the extinction parameter.

A method to derive w_d, v_d and v'_d , and to resolve the differential Eq. (8) is given in (Verhoef, 1985, 1998). Here, we show an alternative method based on the analogy between $L_{d,d}$ and E_o , and deriving $t_{d,d}$ versus ρ_{so} .

Fig. 2 shows the relative orientation of the source, the leaf and the upward/downward observations. Referring to the leaf, the upward and the downward observation directions are symmetric. The contribution of a Lambertian flux scattered by the top of the leaf to the radiance in the upward direction is the same as the contribution of the flux scattered by the bottom of the leaf to the downward direction. Therefore, by just interchanging the leaf ρ and τ , the contribution of an incident flux (direct or diffuse) to the downward direction is deduced from the upward one. Each Eq. (8) scattering parameter ($p_d \in \{w_d, v_d, v'_d\}$) is then derived from the corresponding SAIL one ($p \in \{w, v, v'\}$) as follows:

$$p_d(\theta_d, \varphi_d, \rho, \tau) = \frac{1}{\pi} p(\pi - \theta_d, \pi + \varphi_d, \tau, \rho).$$

By the same way, one has:

$$K_d(\theta_d, \varphi_d) = K(\pi - \theta_d, \pi + \varphi_d).$$

Eq. (8) can be expressed as follows:

$$\frac{dL_{d,d}(z)}{dz} = -g(z) + K_d L_{d,d}(z), \tag{9}$$

with $g(z) = w_d E_s(z) + v_d E_-(z) + v'_d E_+(z)$. The general solution of Eq. (9) is $L_{d,d}(z) = h(z) \exp(K_d z)$, with $h'(z) = -g(z) \exp(-K_d z)$. Using the boundary condition: $L_{d,d}(0) = 0$, we obtain the following expression:

$$L_{d,d}(-1) = \exp(-K_d) \int_{-1}^0 g(z) \exp(-K_d z) dz. \tag{10}$$

Then,

$$t_{d,d}(w_d, v_d, v'_d, K_d) = \frac{\exp(-K_d) \int_{-1}^0 g(z) \exp(-K_d z) dz}{E_s(0)}. \tag{11}$$

Now, similarly the equation of E_o (Verhoef, 1985), one can show that:

$$\rho_{so}(w, v, v', K) = \frac{\int_{-1}^0 g_r(z) \exp(Kz) dz}{E_s(0)}, \quad (12)$$

with $g_r(z) = wE_s(z) + vE_-(z) + v'E_+(z)$. Therefore, introducing Eq. (11) in Eq. (12), we obtain:

$$t_{d,d}(w_d, v_d, v'_d, K_d) = \exp(-K_d) \rho_{so}(w_d, v_d, v'_d, -K_d).$$

Fig. 3 summarizes the layer scattering term estimation presented in this section: r_t , $t_{d,s}$ and $t_{d,d}$. The other layer scattering terms r_b , $t_{u,s}$ and $t_{u,d}$ are respectively equal to r_t , $t_{d,s}$ and $t_{d,d}$. These terms allow the definition of the vegetation layer operators Eq. (2). Using such a model, the operator estimation is not accurate since it depends on E_+ and E_- assumed isotropically distributed over hemispheres. In Section 3, we show a method to overcome this problem. Moreover, we present both the derivation of canopy (soil+several vegetation layers) reflectance and the operator discretization.

2.3. Discrete case: AddingSD

In the discrete case, the leaf size is assumed non-null inducing a non-negligible correlation between the incident flux path and the diffuse flux one. This phenomenon is the well-known hot spot effect (Suits, 1972; Kuusk, 1985, 1991b). In previous studies, the hot spot effect was taken into account in the 1-D model only for the direct fluxes. Now, in this paper we show that not considering this effect for diffuse fluxes leads to radiative budget violation, and hence we propose to treat all fluxes similarly.

To understand these two phenomena (energy conservation/multi hot spot), we consider Fig. 4. It shows a configuration of a vegetation layer composed of two sublayers 1 and 2. The direct flux (solid line in black) is scattered only by a leaf (M), whereas the gray flux (respectively the black dashed flux) is also scattered by leaves in the layer 2 before (respectively only after) scattering by M . Kuusk' model takes into account the correlation between direct fluxes ($N_1 \rightarrow M \rightarrow N_2$) by increasing the amount of the corresponding flux exiting the vegetation layer (from N_2). However this increase is not accompanied by a decrease of diffuse fluxes (decrease due to absence of interaction between the direct flux and the vegetation components, e.g. decrease of fluxes reaching T_1 and R_3). Furthermore, such a modeling does not take into account the correlations between diffuse fluxes (e.g. $R_1 \rightarrow M \rightarrow R_2$). In the following this phenomenon is called the 'multi hot spot' effect.

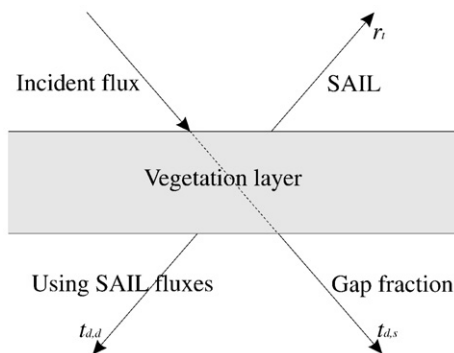


Fig. 3. Vegetation layer scattering term estimation: r_t is estimated by the SAIL model, $t_{d,s}$ is estimated according to the gap fraction, and $t_{d,d}$ is derived from the SAIL model formalism.

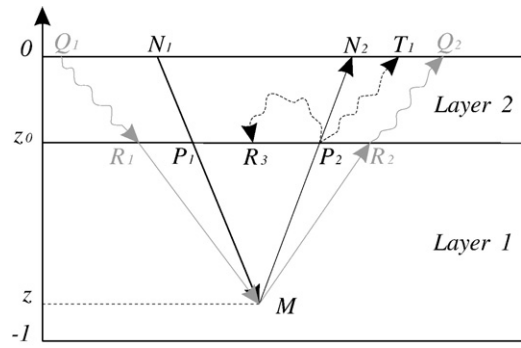


Fig. 4. Two successive vegetation layers 1 and 2 such that the layer 2 is thin and the leaf radius is not null. The depth of the two layers equals 1. Two incident fluxes reaching the top of the canopy are scattered by a leaf M . The difference between the two fluxes is that the gray one is also scattered in the layer 2 before scattering by M . The dashed flux is collided by vegetation in layer 2 after scattering by M .

In this section, we first recall the Kuusk model from (Kuusk, 1985, 1991b). Then, we present our approach: the AddingSD model.

2.3.1. Kuusk model

Now, let us only deal with the direct flux, the corresponding reflectance is called the single reflectance $\rho_{HS}^{(1)}$ (the corresponding radiance is called $L_{o,HS}^{(1)}$). The source and observation directions are respectively Ω_s and Ω_o . From (Verhoef, 1998, pp 150–159), $\rho_{HS}^{(1)}(z)$ can be expressed as follows:

$$\rho_{HS}^{(1)}(z) = P_{so}(\Omega_s, \Omega_o, z) \frac{w}{\pi}, \quad (13)$$

where w is the SAIL model bidirectional volume scattering coefficient for vegetation components [(Verhoef, 1984); assuming a vegetation layer architecture, this term is exact: it does not depend on the diffuse fluxes], and $P_{so}(\Omega_s, \Omega_o, z)$ is the joint probability that the incident flux reaches M without any collision with other canopy components and that, after scattering by M , it also reaches the top of the canopy without any collision with the vegetation. In a turbid medium the two probabilities being independent,

$$P_{so}(\Omega_s, \Omega_o, z) = P_s(\Omega_s, z) P_o(\Omega_o, z), \quad (14)$$

with $P_s(\Omega_s, z) = \exp(kz)$, $P_o(\Omega_o, z) = \exp(Kz)$, k and K are respectively the extinctions in the source and observation directions. However, for discrete leaves, they are dependent, and one obtains (Kuusk, 1985; Verhoef, 1998):

$$P_{so}(\Omega_s, \Omega_o, z) = \exp[(K + k)z] C_{HS}(\Omega_s, \Omega_o, z), \quad (15)$$

with C_{HS} the correction factor referring to the independent case Eq. (14):

$$C_{HS}(\Omega_s, \Omega_o, z) = \exp\left\{ \sqrt{kK} \frac{1}{b} [1 - \exp(bz)] \right\}, \quad (16)$$

with b is a complex term depending on the hot spot parameter (d_i) defined as the ratio between the mean leaf radius and the height of the vegetation layer.

Now, in the AddingSD model, the first order hot spot effect is modeled as follows: for a layer located at an altitude between -1 and 0 , a direction of source Ω_s , a direction of observation Ω_o and an element M located at $z < 0$:

$$\rho_{HS}^{(1)}(z) = \rho^{(1)}(z) C_{HS}(\Omega_s, \Omega_o, z), \quad (17)$$

with $\rho^{(1)}$ the single scattering reflectance in the independent case Eq. (14).

Considering only the first order hot spot effect, one computes the canopy BRDF in the turbid case, and then adds the difference between $\rho_{HS}^{(1)}$ and $\rho^{(1)}$. However, in this case, the energy would no longer be conserved.

The following subsection presents the way we compute the hot spot also for diffuse fluxes, and the energy conservation can be satisfied.

2.3.2. Multi hot spot model

Firstly we assume that the energy conservation is insured by the AddingS model whatever be the vegetation parameter LAI (property shown later, cf. Section 4.1). In this subsection, we first show that modifying $\rho^{(1)}$ (replaced by $\rho_{HS}^{(1)}$) corresponds to the use of a fictive equivalent LAI, called LAI_{HS}. Clearly, using LAI_{HS} for $\rho^{(1)}$ and LAI_{actual} for the high order reflectances and transmittances, respectively called $\rho^{(n)}$ and $\tau^{(n)}$, $n > 1$ (where n is the number of the flux collisions) does not lead to energy conservation.

The following of the subsection is organized as follows: first we define $P_0(\Omega_0|\Omega_s, z_0, z)$ from which we will propose an estimation of LAI_{HS}. Then, we derive $\rho^{(n)}$ and $\tau^{(n)}$, $n > 1$, and the Adding operators using LAI_{HS}. Finally, we show that the diffuse fluxes can be handled similarly to the direct flux since the Adding method provide equivalent direct fluxes in output of the sublayers. The bidirectional scattering terms will be used to define the Adding method operators of the model AddingSD.

Dividing the part of the layer from top to the depth z into n_{sub} small sublayers having depth $\Delta z = \frac{|z|}{n_{sub}}$, the joint probability that both fluxes are free of collisions with the sublayer i , called $P_{s_0,i}(\Omega_s, \Omega_0, z, \Delta z)$, is (Kuusk, 1985):

$$P_{s_0,i}(\Omega_s, \Omega_0, z, \Delta z) = \exp \left[- \left\{ K + k - \sqrt{Kk} \exp \left[\left(1 - \frac{i}{n_{sub}} \right) bz \right] \right\} \Delta z \right]. \quad (18)$$

Now, for a given sublayer i , we define the conditional probability that the flux in the direction Ω_0 does not collide with leaves given the same property for the incident flux, it is called $P_{0,i}(\Omega_0|\Omega_s, z, \Delta z)$:

$$P_{0,i}(\Omega_0|\Omega_s, z, \Delta z) = \frac{P_{s_0,i}(\Omega_s, \Omega_0, z, \Delta z)^2}{P_{s,i}(\Omega_s, z, \Delta z)}, \quad (19)$$

where $P_{s,i}(\Omega_s, z, \Delta z)$ represents the prior gap probability in the direction Ω_s .

Since $P_{s,i}(\Omega_s, z, \Delta z) = \exp[-k\Delta z]$, then according to Eq. (19):

$$P_{0,i}(\Omega_0|\Omega_s, z, \Delta z) = \exp \left[- \left\{ K - \sqrt{Kk} \exp \left[\left(1 - \frac{i}{n_{sub}} \right) bz \right] \right\} \Delta z \right]. \quad (20)$$

The posterior probability that the flux does not collide with leaves when exiting the layer 2 ($z' \in [z_0, 0]$) in direction Ω_0 given that the incident flux does not collide with leaves in the layer 2 in direction Ω_s is called $P_0(\Omega_0|\Omega_s, z_0, z)$. From Eq. (20), and inspiring from Kuusk (1985), it is straightforward to show:

$$P_0(\Omega_0|\Omega_s, z_0, z) = \exp \left[- \int_{z_0}^0 \left\{ K - \sqrt{Kk} \exp[(z-x)b] \right\} dx \right], \\ = \exp[Kz_0] C_{HS}(\Omega_s, \Omega_0, z_0, z).$$

with C_{HS} the generalized correction factor:

$$C_{HS}(\Omega_s, \Omega_0, z_0, z) = \exp \left\{ \sqrt{kK} \frac{1}{b} (\exp[b(z-z_0)] - \exp[bz]) \right\}. \quad (21)$$

Note that $C_{HS}(\Omega_s, \Omega_0, z) = C_{HS}(\Omega_s, \Omega_0, z, z)$ and:

$$C_{HS}(\Omega_s, \Omega_0, z) = C_{HS}(\Omega_s, \Omega_0, z-z_0) C_{HS}(\Omega_s, \Omega_0, z_0, z). \quad (22)$$

In the case of the direct flux (in black and solid in Fig. 4), the first order contribution of the leaf M to the layer BRDF is given by:

$$\rho_{HS}^{(1)}(z) = \frac{W}{\pi} \exp[(k+K)z] C_{HS}(\Omega_s, \Omega_0, z), \\ = \frac{W}{\pi} \exp[(k+K)(z-z_0)] C_{HS}(\Omega_s, \Omega_0, z-z_0) \\ \exp[kz_0] \exp[Kz_0] C_{HS}(\Omega_s, \Omega_0, z_0, z), \quad (23) \\ = \underbrace{\exp[kz_0]}_{P_s(\Omega_s, z_0)} \underbrace{\rho_{HS}^{(1)}(z-z_0)}_{P_1 \rightarrow M \rightarrow P_2} \underbrace{\exp \left\{ \overbrace{Kz_0 + \log[C_{HS}(\Omega_s, \Omega_0, z_0, z)]}^{K_{HS}(\Omega_0|\Omega_s, z_0, z) z_0} \right\}}_{P_0(\Omega_0|\Omega_s, z_0, z)},$$

From the last equality of Eq. (23), $\rho_{HS}^{(1)}(z)$ can be interpreted as follows: reaching the top of the canopy the direct flux is partially extinguished in the layer 2 by the factor $P_s(\Omega_s, z_0)$ (from N_1 to P_1). Then, reaching the interface between the two layers at P_1 , its amplitude will be determined according to $\rho_{HS}^{(1)}(z-z_0)$ that depends on the layer 1 features (from P_1 to P_2 , passing through M). Finally, $K_{HS}(\Omega_0|\Omega_s, z_0, z)$ can be viewed as the ‘effective’ extinction related to the conditional probability of gap $P_0(\Omega_0|\Omega_s, z_0, z)$ of the layer 2 (from P_2 to N_2). Indeed, $K_{HS} < K$ means that the probability of collision with leaves for $L_{0,HS}^{(1)}$ is decreased. Since the extinction depends linearly on LAI, one can deem that LAI is locally decreased by the factor $\gamma = \frac{K_{HS}}{K}$:

$$LAI_{HS}(\Omega_0|\Omega_s, z_0, z) = \frac{K_{HS}(\Omega_0|\Omega_s, z_0, z)}{K} LAI. \quad (24)$$

The physical interpretation of LAI_{HS} is as follows. Assume that the probability of gap (for a given flux) is increased in the layer 2. For this flux, the ‘effective’ density of vegetation encountered when crossing the layer is reduced accordingly. Obviously, the first collision between the flux and the vegetation is reduced according to the same density of vegetation. Now, since the layer 2 is thin, its corresponding reflectance and diffuse transmittance depend mainly on the first interaction. So, just an approximation of the multiple scattered fluxes is sufficient to derive the layer 2 scattering terms with good accuracy. For that, the derivation of all diffuse fluxes can be done using this ‘effective’ density of vegetation (LAI_{HS} in our case). Moreover, for such a modeling, the interactions of the considered flux and the layer 2 components (transmittance by extinction, reflectance and diffuse transmittance) are derived using exactly the same LAI value (LAI_{HS}), which is physically consistent and thus leads to the conservation of the energy of this flux. Furthermore, by doing the same processing for all fluxes exiting the layer 1 in direction of the layer 2, the energy of all fluxes is conserved and so the energy is conserved in the system composed by the two vegetation layers.

Here we propose that, consequently, in the layer 2, the reflectance and diffuse transmittance of the flux $L_{0,HS}^{(1)}$ are calculated using the ‘effective’ density LAI_{HS}. They are respectively called $r_{b,2,HS}(\Omega_s, z, \Omega_0 \rightarrow \cdot)$ (from P_2 to R_3) and $t_{d,2,HS}(\Omega_s, z, \Omega_0 \rightarrow \cdot)$ (from P_2 to T_1). In summary, we view the multi hot spot effect as a local reduction of the LAI in the layer 2.

Fig. 5 shows the recursive construction of the multi hot spot effect for a given vegetation layer. The considered layer is divided into 4 thin sublayers. The multi hot spot effect construction begins from two sublayers, chosen sufficiently thin so that the leaves do not overlap and so the hot spot effect does not occurs within a sublayer. Now, for two sublayers, the first order hot spot effect is computed between sublayers (it corresponds to a local decrease of the LAI, represented by dark gray ellipse). In addition to the first order hot spot effect, when a third sublayer is added, a hot spot effect is computed in the sublayers 1+2 for flux scattered in the sublayer 3 (cf. Fig. 5b second case). In the case of four sublayers

² The conditional probability of ‘A’ given ‘B’, noted $P(A|B)$, is equal to $\frac{P(A,B)}{P(B)}$.

³ Use Eq. (22) to separate C_{HS} .

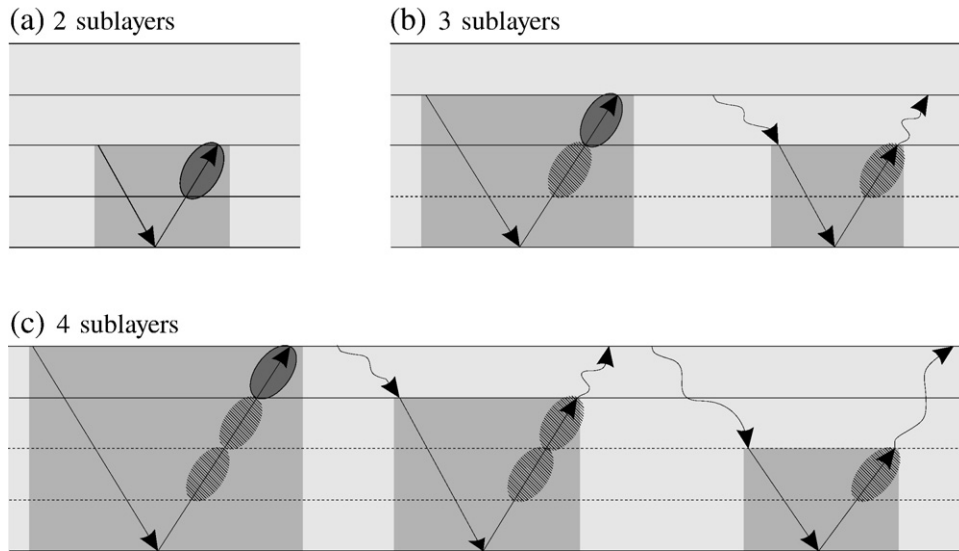


Fig. 5. Multi hot spot effect construction for a vegetation layer composed by 4 sublayers. The dark gray rectangles show the first order hot spot effect, the dark gray ellipses show the local reduction of LAI and the dashed ellipses show the local reduction of LAI taken into account previously. Sublayers separated by dashed lines are considered as a single layer (in Fig. 4, it corresponds to the layer 1 and the sublayer just above is considered as the layer 2). For 2 sublayers, we consider only the hot pot effect, besides for 3 and 4 sublayers, the hot spot between diffuse fluxes is taken into account.

(Fig. 5c), the hot spot for fluxes scattered in the sublayer 4 and the sublayers 3+4 is computed respectively in the sublayers 1+2+3 (cf. Fig. 5c second case) and the sublayers 1+2 (cf. Fig. 5c third case). Using such a modeling, we take into account the hot spot effect for any flux scattered in any sublayer of a vegetation layer, in the vegetation located below. Hence the name, multi hot spot effect.

Note that, in the following, the sublayer LAI is called L_{HS} . L_{HS} is higher than the elementary sublayer LAI (L_{min}).

In summary, the hot spot is treated as follows: we begin by a thin sublayer, and we add each time a new thin sublayer. The already concatenate sublayers and the new sublayer are respectively equivalent to the layer 1 and 2 of Fig. 4. The concatenation of the thin layer is deferent to the classical adding principle only for the three fluxes $N_1 \rightarrow P_1 \rightarrow M \rightarrow P_2 \rightarrow N_2$, $N_1 \rightarrow P_1 \rightarrow M \rightarrow P_2 \rightarrow T_1$ and $N_1 \rightarrow P_1 \rightarrow M \rightarrow P_2 \rightarrow R_3$.

3. Implementation

In this section, we present the implementation of the coupled model Adding/SAIL in the turbid and the discrete case: AddingS and AddingSD. In the turbid case, the AddingS model is based on the Adding principle: concatenation of many layers. Moreover, this principle is adapted to the discrete case (AddingSD model) by distinguishing between fluxes scattered once and those scattered

many times. In this section, we present firstly the Adding method principle, then we expose the AddingS model algorithm. After that, we show successively the operator derivation and the algorithm of the AddingSD model.

3.1. Adding method computation principle

Here, we first show the basic of the computation of the Adding method: derivation the Adding operators for multiple vegetation layers given the operators of each one. Then, we present a new formulation of medium operators.

3.1.1. Multiple layer operators

Assuming a vegetation canopy represented by some horizontal layers covering the soil, the relationship between the output flux and the input flux reaching the canopy may be described by layer operators. Fig. 6 illustrates the four terms: \mathcal{R}_t , \mathcal{R}_b , \mathcal{T}_u and \mathcal{T}_d , respectively representing the reflectance operators of the top and bottom of the layer and the transmittance operators upward and downward. Defining the interface between the soil and the vegetation layer, Fig. 6 shows the interactions between two successive layers: at the interface, the radiation incident from layer 2 on layer 1 is either absorbed, transmitted downward or reflected upward by layer 2, and then either transmitted or reflected by layer 1, and so on.

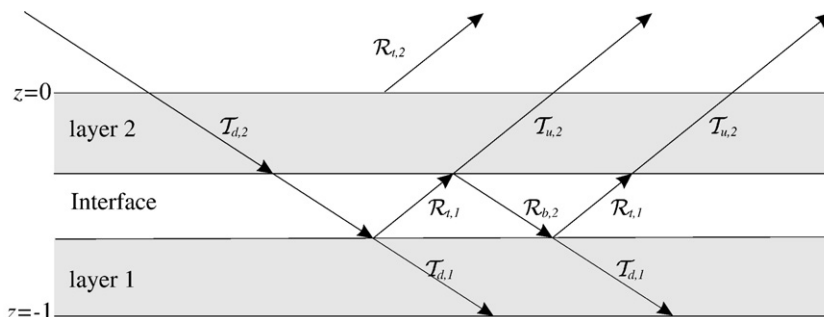


Fig. 6. Adding method: Multi-interactions between two successive layers. The scattering operators are \mathcal{R}_t reflectance from the top of layer, \mathcal{R}_b reflectance from the bottom of the layer, \mathcal{T}_u upward transmittance and \mathcal{T}_d downward transmittance. The second subscript denotes the provenance layer of the flux.

In the following, the hemispherical distribution of incident radiance from above the layer 2 is called $L_s(0)$. The energetic budget for the case of only two layers involves the following terms:

- the distribution of radiance ($L_{0,2}$) scattered by the layer 2:

$$L_{0,2} = \mathcal{R}_{t,2}[L_s(0)], \tag{25}$$

where $\mathcal{R}_{t,2}$ is the top reflectance of the layer 2.

- The radiance scattered by the layer 1 ($L_{0,1}$): it is equal to the infinite sum of the fluxes respectively associated to a given number of 'reflection(s)' between the two layers:

$$L_{0,1} = \mathcal{T}_{u,2} \circ (\mathcal{R}_{t,1} + \mathcal{R}_{t,1} \circ \mathcal{R}_{b,2} \circ \mathcal{R}_{t,1} + \mathcal{R}_{t,1} \circ \mathcal{R}_{b,2} \circ \mathcal{R}_{t,1} \circ \mathcal{R}_{b,2} \circ \mathcal{R}_{t,1} + \dots) \circ \mathcal{T}_{d,2}[L_s(0)], \tag{26}$$

$$= \mathcal{T}_{u,2} \circ (I - \mathcal{R}_{t,1} \circ \mathcal{R}_{b,2})^{-1} \circ \mathcal{R}_{t,1} \circ \mathcal{T}_{d,2}[L_s(0)],$$

where $\mathcal{T}_{u,2}$, $\mathcal{T}_{d,2}$ are respectively the upward and downward transmittances of the layer 2, $\mathcal{R}_{t,2}$ and $\mathcal{R}_{b,1}$ are the reflectances of respectively the top of layer 1 and the bottom of layer 2, and I is the identity operator.

Adding Eqs. (25) and (26) leads to:

$$L_0 = L_{0,2} + L_{0,1} = (\mathcal{R}_{t,2} + \mathcal{T}_{u,2} \circ (I - \mathcal{R}_{t,1} \circ \mathcal{R}_{b,2})^{-1} \circ \mathcal{R}_{t,1} \circ \mathcal{T}_{d,2})[L_s(0)]. \tag{27}$$

So, the top reflectance operator for the canopy is given by Verhoef (1985):

$$\mathcal{R}_t = \mathcal{R}_{t,2} + \mathcal{T}_{u,2} \circ (I - \mathcal{R}_{t,1} \circ \mathcal{R}_{b,2})^{-1} \circ \mathcal{R}_{t,1} \circ \mathcal{T}_{d,2}. \tag{28}$$

Similarly, the other operators for two layers are given by Verhoef (1985):

$$\begin{aligned} \mathcal{R}_b &= \mathcal{R}_{b,1} + \mathcal{T}_{d,1} \circ (I - \mathcal{R}_{b,2} \circ \mathcal{R}_{t,1})^{-1} \circ \mathcal{R}_{b,2} \circ \mathcal{T}_{u,1}, \\ \mathcal{T}_d &= \mathcal{T}_{d,1} \circ (I - \mathcal{R}_{b,2} \circ \mathcal{R}_{t,1})^{-1} \circ \mathcal{T}_{d,2}, \\ \mathcal{T}_u &= \mathcal{T}_{u,2} \circ (I - \mathcal{R}_{t,1} \circ \mathcal{R}_{b,2})^{-1} \circ \mathcal{T}_{u,1}, \end{aligned} \tag{29}$$

where the signification of the layer 1 operators $\mathcal{T}_{\cdot,1}$ and $\mathcal{R}_{\cdot,1}$ are the same as $\mathcal{T}_{\cdot,2}$ and $\mathcal{R}_{\cdot,2}$.

Note that here we only present the simple case of two layers. In the general case, more layers can be considered, so the fluxes reaching layer 2 can be transmitted to layer 3, which will scatter them, and so on. Using Eqs. (28) and (29) recursively from the bottom to the top allows the estimation of different canopy operators.

3.1.2. Discretization

In this subsection, we present a discretization of the Adding operators as matrices relating the discrete density of radiant flux in input and in output.

In general case, r , t , L_i and L_e depend on the zenithal and azimuthal angles. Thus, the zenithal angle θ and azimuthal angle φ were sampled respectively into N and M intervals $\Delta\theta_n$ and $\Delta\varphi_m$ respectively centered on θ_n and φ_m with $n \in \{1, \dots, N\}$ and $m \in \{1, \dots, M\}$, the corresponding solid angle is noted $\Omega_{n,m}$. Since $d\Omega = \sin(\theta)d\theta d\varphi$, then $\Delta\Omega_{n,m} = \sin(\theta_n)\Delta\theta_n\Delta\varphi_m$. Moreover, as $dE(\Omega) = L(\Omega)\cos(\theta)d\Omega$, then

$$\Delta E(\Omega_{n,m}) = L(\Omega_{n,m}) \cos(\theta_n)\Delta\Omega_{n,m} = L(\Omega_{n,m}) \cos(\theta_n) \sin(\theta_n)\Delta\theta_n\Delta\varphi_m. \tag{30}$$

$$\begin{aligned} \mathcal{R}[L_i](\Omega_e) &= \int_0^{2\pi} \int_0^{\pi/2} r(\Omega_i \rightarrow \Omega_e)L_i(\Omega_i) \cos(\theta_i) \sin(\theta_i)d\theta_i d\varphi_i, \\ &\approx \sum_{l_\varphi=1}^M \sum_{l_\theta=1}^N r(\Omega_{i;l_\theta,l_\varphi} \rightarrow \Omega_e)L_i(\theta_{i;l_\theta}) \cos(\theta_{i;l_\theta}) \sin(\theta_{i;l_\theta}) \Delta\theta_{i;l_\theta} \Delta\varphi_{i;l_\varphi}, \\ &\approx \sum_{l_\varphi=1}^M \sum_{l_\theta=1}^N r(\Omega_{i;l_\theta,l_\varphi} \rightarrow \Omega_e)E_i(\Delta\Omega_{i;l_\theta,l_\varphi})^4 \end{aligned}$$

⁴ Use Eq. (30).

By the same way, the outward zenithal angle θ_e and the outward azimuthal angle φ_e were sampled respectively into N and M intervals $\Delta\theta_{e,k_\theta}$ and $\Delta\varphi_{e,k_\varphi}$ respectively centered on θ_{e,k_θ} and φ_{e,k_φ} . The following relationship between $E_i(\Delta\Omega_{i;l_\theta,l_\varphi})$ and $E_e(\Delta\Omega_{e;k_\theta,k_\varphi})$ is obtained:

$$\begin{aligned} E_e(\Delta\Omega_{e;k_\theta,k_\varphi}) &= \cos(\theta_{e,k_\theta}) \sin(\theta_{e,k_\theta}) \Delta\theta_{e,k_\theta} \Delta\varphi_{e,k_\varphi} \sum_{l_\varphi=1}^M \sum_{l_\theta=1}^N r(\Omega_{i;l_\theta,l_\varphi} \rightarrow \Omega_{e;k_\theta,k_\varphi}) E_i(\Delta\Omega_{i;l_\theta,l_\varphi}). \end{aligned} \tag{31}$$

By considering the indices $l=N(l_\varphi-1)+l_\theta$ and $k=N(k_\varphi-1)+k_\theta$, Eq. (31) becomes:

$$E_e(\Delta\Omega_{e,k}) = \cos(\theta_{e,k}) \Delta\Omega_{e,k} \sum_{l=1}^{MN} r(\Omega_{i,l} \rightarrow \Omega_{e,k}) E_i(\Delta\Omega_{i,l}). \tag{32}$$

So, a matrix form of the discretized reflectance operator is derived:

$$R(l, k) = r(\Omega_{i,l} \rightarrow \Omega_{e,k}) \cos(\theta_{e,k}) \Delta\Omega_{e,k}, \tag{33}$$

R is a $NM \times NM$ matrix. By the same way, we derive the matrix form transmittance operator:

$$T(l, k) = t(\Omega_{i,l} \rightarrow \Omega_{e,k}) \cos(\theta_{e,k}) \Delta\Omega_{e,k}. \tag{34}$$

Finally, for a discrete density of irradiant input flux E_i (vector of samples) the output density of radiant flux E_e is given by:

$$E_e = O E_i, \tag{35}$$

where O equals R for the reflectance case and T for the transmittance case.

Using matrix operators, Eq. (28) becomes

$$\mathcal{R}_t = \mathcal{R}_{t,2} + \mathcal{T}_{u,2} (I - \mathcal{R}_{t,1} \mathcal{R}_{b,2})^{-1} \mathcal{R}_{t,1} \mathcal{T}_{d,2}, \tag{36}$$

where the signification of the subscripts in the R and T matrix expression is the same as in the case of \mathcal{R} and \mathcal{T} .

In this study, we opt to regular discretization of the azimuthal angle ensuring a zenithal invariance by rotation, i.e.:

$$\begin{aligned} r(\Omega_{i;l_\theta,l_\varphi+q} \rightarrow \Omega_{e;k_\theta,k_\varphi+q}) &= r(\Omega_{i;l_\theta,l_\varphi} \rightarrow \Omega_{e;k_\theta,k_\varphi}), \forall l_\theta, k_\theta \in \{1, \dots, N\}, l_\varphi, k_\varphi, q \in \{1, \dots, M\}. \end{aligned}$$

So, we have only to compute only $M \times N^2$ terms. In the case, when such an invariance property is not needed, other hemispherical samplings (quadratures) could be proposed when more adapted to the considered application: for example in the Discrete-Ordinates Method (DOM), many other optimized quadratures have been used (Kokhanovsky, 2007).

The reflectance and the diffuse transmittance operators are simple to estimate since for each layer the values of $r(\Omega_{i,l} \rightarrow \Omega_{i,k})$, $t_{u,d}(\Omega_{i,l} \rightarrow \Omega_{i,k})$ and $t_{d,s}(\Omega_s \rightarrow \Omega_o)$ are computed. Now, as in the formulation of the transmittance by extinction, there are Dirac functions. The corresponding operator is derived as follows. Recall that

$$t_{d,s}(\Omega_s \rightarrow \Omega_o) = \frac{\tau_{ss} \delta(\theta = \theta_s) \delta(\varphi = \varphi_s)}{\cos(\theta_s) \sin(\theta_s)}.$$

For given discretizations of the zenithal and azimuthal angles $\{\theta_1, \dots, \theta_N\}$ and $\{\varphi_1, \dots, \varphi_M\}$, let us define the simple functions:

$$\begin{cases} q_\theta : [0, \pi/2] \rightarrow \{1, \dots, N\}, \\ q_\theta(\theta) = \operatorname{argmin}_{n \in \{1, \dots, N\}} |\theta - \theta_n|, \end{cases} \text{ and } \begin{cases} q_\varphi : [0, 2\pi] \rightarrow \{1, \dots, M\}, \\ q_\varphi(\varphi) = \operatorname{argmin}_{m \in \{1, \dots, M\}} |\varphi - \varphi_m|. \end{cases} \tag{37}$$

⁵ $\theta \in [\theta_n - \frac{\Delta\theta_n}{2}, \theta_n + \frac{\Delta\theta_n}{2}]$.
⁶ $\varphi \in [\varphi_m - \frac{\Delta\varphi_m}{2}, \varphi_m + \frac{\Delta\varphi_m}{2}]$.

$\delta(\theta=\theta_s)$ and $\delta(\varphi=\varphi_s)$ can be approximated respectively as follows,

$$\begin{cases} \frac{1}{\Delta\theta_{e,k}}, & \text{if } q_\theta(\theta) = q_\theta(\theta_s), \\ 0, & \text{otherwise,} \end{cases} \quad \text{and} \quad \begin{cases} \frac{1}{\Delta\varphi_{e,k}}, & \text{if } q_\varphi(\varphi) = q_\varphi(\varphi_s), \\ 0, & \text{otherwise.} \end{cases}$$

The discrete $t_{d,s}$ can be assumed constant over the solid angle $\Delta\Omega_{e,k}$:

$$\begin{cases} t_{d,s}(\Omega_{i,l} \rightarrow \Omega_{e,k}) = \frac{\tau_{ss}(\Omega_{e,k})}{\cos(\theta_{e,k})\Delta\Omega_{e,k}}, & \text{if } l = k, \\ = 0, & \text{otherwise,} \end{cases} \Rightarrow \begin{cases} T_{d,s}(l,k) = \tau_{ss}(\Omega_{e,k}), & \text{if } l = k, \\ = 0, & \text{otherwise,} \end{cases}$$

where $T_{d,s}$ is the discrete downward transmittance operator by extinction which corresponds to a diagonal matrix.

By discretization, the BRDF is computed only for a finite number of samples. In order to compute the radiance in arbitrary directions, and since the BRDF is more sensitive to the zenithal angle variation than to the azimuthal angle variations, then linear interpolation is applied in the zenith domain, and nearest neighbor interpolation in the azimuth domain.

Note finally that, by discretization of Eqs. (28) and (29), the different layer operators become matrices, the ‘ \circ ’ operator becomes matrix multiplication and the input/output distributions become irradiance vectors. Such discrete equations were also presented in Verhoef (1985, 1998). However, in this previous work, a separation was made between source and observed fluxes from the others. As it will be shown in Section 3.3, and for the flux scattered one time by the vegetation (or by the soil), such a separation can be taken into account in the AddingS and AddingSD models.

3.2. AddingS algorithm

In the turbid case, using the bidirectional reflectance and transmittance derivation presented in section (2.2), one can derive the discrete operators for a vegetation according to layer Eqs. (33) and (34). However, this method gives poor results for very dense layer, since at the bottom the direct flux becomes negligible compared to the diffuse fluxes assumed isotropical. Then, the percentage in the total amount of radiance in the direction of observation provided by diffuse fluxes increases. As these fluxes are assumed isotropically distributed over the hemispheres, the performance of the bidirectional reflectance and transmittance as well as their corresponding operator estimation decreases.

Note that, to overcome the assumption of semi-isotropic diffuse fluxes, Verhoef (1998, 2002) proposed to discretize the diffuse fluxes into 72 subfluxes, turning the SAIL equations into a matrix–vector equation. Moreover, the well-known Discrete-Ordinates Method (DOM) does not consider any assumption over diffuse fluxes (Chandrasekhar, 1950). DOM divides the radiant flux into subfluxes and using the Legendre Polynomials tries to solve the radiative transfer equation over a mesh cells (set of couples: altitude and discrete solid angle).

Here, in the AddingS model, we propose to divide each vegetation layer into small sublayers, for each of them the operators are estimated, after that using the Adding principle (presented in Section 3.1.1) recursively we derive the initial layer operators. Indeed, for small depth layers, the diffuse fluxes provided by the interaction between the incident flux and the different layer elements are negligible compared to the incident flux. Therefore, for such a configuration, the output fluxes can be computed in an accurate way under the isotropic diffuse flux assumption. Experimental results show that the model stability is reached for diffuse irradiances lower than 5% of total irradiance. In general, sublayer $L_{min} = 10^{-2}$ is sufficient to reach stability.

Note that, DOM consists also to divide the whole layer into thin layers. The difference between DOM and the AddingS model is that DOM use differential operators in each mesh, whereas AddingS considers the relationships between input and output fluxes of an elementary layers and using the Adding principle the relationships between input/output fluxes for a thick layer are determined.

The different operator elements are estimated for the sublayer with depth L_{min} . Then, according to the Adding method principle Eqs. (28) and (29), they are deduced for $2L_{min}$, and for $4L_{min}$ noting that $4L_{min} = 2(2L_{min})$, and so on. Having estimated the operators for any sublayer of depth $2^i L_{min}$, the operators for a vegetation layer of depth L are obtained decomposing L as $\sum_{i=0}^n a_i 2^i L_{min}$, with $a_i \in \{0,1\}$ (within about L_{min}). The layer operators are then calculated by considering the sublayers $2^i L_{min}$ with $a_i = 1$. Such a dividing allows the acceleration of the layer operator derivation: about $\log_2(L/L_{min})$ operations (an operation corresponds to the computation of the four layer operators, Eqs. (28) and (29)) are required, whereas if at each time only one sublayer was added, L/L_{min} operations would be required.

Fig. 7 shows an example of derivation of the AddingS layer operators. The layer is decomposed into 8 thin layers. Using the decomposition on powers of 2 ($8 = 1 \times 2^3 + 0 \times 2^2 + 0 \times 2^1 + 0 \times 2^0$), only $a_3 \neq 0$. Therefore it is sufficient to apply the Adding method 3 times: $2L_{min}$, $2^2 L_{min}$ and $2^3 L_{min}$.

So, we have an analytical expression of the AddingS model parameters in the case of one vegetation layer. Then, we can derive the top and bottom reflectance and upward and downward transmittance matrix operators according to Eqs. (33) and (34). By combining them with the soil reflectance operators (by assuming that it is a Lambertian surface or by using the soil bidirectional reflectance model of Hapke (1981)) we can obtain the canopy reflectance.

3.3. AddingSD operator derivation

The development presented in this section is based on the case of the two layers presented in Fig. 4. We aim at deriving the AddingSD global reflectance and transmittance operators for the two vegetation layers presented in Fig. 4. For this, we vary $M(z)$ and estimate the different LAI_{HS} , $r_{b,2,HS}$ and $t_{d,2,HS}$. Unfortunately, doing this, model operators will no longer be separable, and thus we are only able to compute an equivalent combination of these operators.

Note that, in this section and as explained in Section 2.2, we do not make distinction between downward and upward transmittances ($T_d = T_u = T$). But, we make distinction between different kinds of

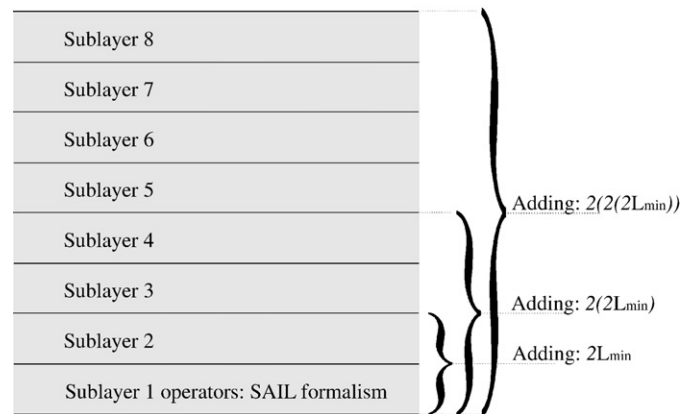


Fig. 7. AddingS vegetation layer operator estimation: the layer is divided into 8 thin sublayers for which the operators are estimated using the SAIL formalism. After that the operators of 2, 4 and 8 sublayers are derived using the Adding principle.

transmittance, either by extinction (\mathcal{T}_s) or by diffusion (\mathcal{T}_d). In particular, for the layer 2, one has:

$$\mathcal{T}_{d,2} + \mathcal{T}_{u,2} = \mathcal{T}_2 = \mathcal{T}_{s,2} + \mathcal{T}_{d,2}. \quad (38)$$

As explained in Figs. 4 and 5, when a new thin layer is added (layer 2 in Fig. 4), the hot spot effect (first or high order) that should be estimated corresponds to fluxes scattered only one time in the layers already concatenated (Fig. 4, only the leaf M in the layer 1). Therefore, a distinction between multiple scattered fluxes and single scattered flux should be made. Then, let us define firstly the reflectance operator provided from the scattering of the direct flux and the reflectance provided from the multiple scattering. They are called respectively $\mathcal{R}^{(1)}$ (the associated BRDF is called $r^{(1)}$) and $\mathcal{R}^{(mul)}$. In particular, for the layer 1, on has:

$$\mathcal{R}_{t,1} = \mathcal{R}_{t,1}^{(1)} + \mathcal{R}_{t,1}^{(mul)}. \quad (39)$$

Moreover and also according to Fig. 4, the new layer (layer 2) processes differently the flux provided by single reflectance from the layer 1 only if it is transmitted downward by extinction (without making contact with the layer 2 components, $N_1 \rightarrow P_1$). More precisely, let us consider the incident flux from above of the layer 2, if it follows the path $N_1 \rightarrow P_1 \rightarrow M \rightarrow P_2$ (corresponding operator $\mathcal{R}_{t,1}^{(1)} \circ \mathcal{T}_{s,2}$), it will be processed differently by the layer 2 (dark gray ellipse in Fig. 5) according one of the three following cases:

- Transmittance by extinction (first order hot spot, $N_1 \rightarrow P_1 \rightarrow M \rightarrow P_2 \rightarrow N_2$), the corresponding operator ($\mathcal{R}_{t,1} \mathcal{T}_{ss,2}$) is given in the turbid case by

$$\mathcal{R}_{t,1} \mathcal{T}_{ss,2} = \mathcal{T}_{s,2} \circ \mathcal{R}_{t,1}^{(1)} \circ \mathcal{T}_{s,2},$$

- Diffuse transmittance ($N_1 \rightarrow P_1 \rightarrow M \rightarrow P_2 \rightarrow T_1$), the corresponding operator ($\mathcal{R}_{t,1} \mathcal{T}_{sd,2}$) is given in the turbid case by

$$\mathcal{R}_{t,1} \mathcal{T}_{sd,2} = \mathcal{T}_{d,2} \circ \mathcal{R}_{t,1}^{(1)} \circ \mathcal{T}_{s,2},$$

- Reflectance ($N_1 \rightarrow P_1 \rightarrow M \rightarrow P_2 \rightarrow R_3$), the corresponding operator ($\mathcal{R}_{1,2} \mathcal{T}_{s,2}$) is given in the turbid case by

$$\mathcal{R}_{1,2} \mathcal{T}_{s,2} = \mathcal{R}_{b,2} \circ \mathcal{R}_{t,1}^{(1)} \circ \mathcal{T}_{s,2}.$$

In order to separate the first order scattering of diffuse fluxes from the higher orders, we write:

$$\begin{aligned} (I - \mathcal{R}_{t,1} \circ \mathcal{R}_{b,2})^{-1} &= \sum_{i=0}^{+\infty} (\mathcal{R}_{t,1} \circ \mathcal{R}_{b,2})^i = I + \sum_{i=1}^{+\infty} (\mathcal{R}_{t,1} \circ \mathcal{R}_{b,2})^i, \\ &= I + \left(\sum_{i=0}^{+\infty} (\mathcal{R}_{t,1} \circ \mathcal{R}_{b,2})^i \right) \circ \mathcal{R}_{t,1} \circ \mathcal{R}_{b,2}, \\ &= I + (I - \mathcal{R}_{t,1} \circ \mathcal{R}_{b,2})^{-1} \circ \mathcal{R}_{t,1} \circ \mathcal{R}_{b,2}. \end{aligned}$$

According to Eq. (28) and using the equalities (38) and (39), the reflectance of the two layers ($\mathcal{R}_t^{1,2}$) can be written as follows:

$$\begin{aligned} \mathcal{R}_t^{1,2} &= \mathcal{R}_{t,2} + (\mathcal{T}_{s,2} + \mathcal{T}_{d,2}) \circ \left(I + (I - \mathcal{R}_{t,1} \circ \mathcal{R}_{b,2})^{-1} \circ \mathcal{R}_{t,1} \circ \mathcal{R}_{b,2} \right) \\ &\quad \circ \left(\mathcal{R}_{t,1}^{(1)} + \mathcal{R}_{t,1}^{(mul)} \right) \circ (\mathcal{T}_{s,2} + \mathcal{T}_{d,2}), \\ &= \mathcal{T}_{d,2} \circ (I - \mathcal{R}_{t,1} \circ \mathcal{R}_{b,2})^{-1} \circ \underbrace{\mathcal{R}_{t,1} \circ \mathcal{R}_{b,2} \circ \mathcal{R}_{t,1}^{(1)} \circ \mathcal{T}_{s,2}}_{\mathcal{R}_{1,2} \mathcal{T}_{s,2}} + \underbrace{\mathcal{T}_{s,2} \circ \mathcal{R}_{t,1}^{(1)} \circ \mathcal{T}_{s,2}}_{\mathcal{R}_{t,1} \mathcal{T}_{ss,2}} \\ &\quad + \underbrace{\mathcal{T}_{d,2} \circ \mathcal{R}_{t,1}^{(1)} \circ \mathcal{T}_{s,2}}_{\mathcal{R}_{t,1} \mathcal{T}_{sd,2}} + \mathcal{R}_{t,1}^{1,2}, \end{aligned}$$

with $\mathcal{R}_{t,1}^{1,2}$ the sum of the terms not depending on $\mathcal{R}_{t,1}^{(1)} \circ \mathcal{T}_{s,2}$ (in particular those depending on $\mathcal{R}_{t,1}^{(mul)}$).

Note that, not taking into account the hot spot effect, the terms $\mathcal{R}_{t,1} \mathcal{T}_{ss,2}$, $\mathcal{R}_{t,1} \mathcal{T}_{sd,2}$ and $\mathcal{R}_{1,2} \mathcal{T}_{s,2}$ are separable.

Similarly, the downward transmittance of the two layers ($\mathcal{T}_d^{1,2}$) is given by:

$$\mathcal{T}_d^{1,2} = \mathcal{T}_{d,1} \circ (I - \mathcal{R}_{b,2} \circ \mathcal{R}_{t,1})^{-1} \circ \underbrace{\mathcal{R}_{b,2} \circ \mathcal{R}_{t,1}^{(1)} \circ \mathcal{T}_{s,2}}_{\mathcal{R}_{1,2} \mathcal{T}_{s,2}} + \mathcal{T}_{t,r}^{1,2},$$

with $\mathcal{T}_{t,r}^{1,2}$ the sum of the terms not depending on $\mathcal{R}_{t,1}^{(1)} \circ \mathcal{T}_{s,2}$.

We derive the expression of $\mathcal{R}_{t,1} \mathcal{T}_{ss,2}$, putting forward the dependance on z :

$$\begin{aligned} \mathcal{R}_{t,1} \mathcal{T}_{ss,2}[L_i](\Omega_e) &= \int_{\Pi} \int_{\Pi} \int_{\Pi} \underbrace{L_i(\Omega_i)}_{\text{Input}} \underbrace{t_{s,2}(\Omega_i \rightarrow \Omega_e)}_{N_1 \rightarrow P_1} \underbrace{r_{t,1}^{(1)}(\Omega_1 \rightarrow \Omega_2)}_{P_1 \rightarrow M \rightarrow P_2} \\ &\quad \underbrace{\cos(\theta_i) \cos(\theta_1) \cos(\theta_2)}_{P_2 \rightarrow N_2} d\Omega_i d\Omega_1 d\Omega_2, \\ &= \int_{\Pi} \int_{\Pi} \int_{\Pi} L_i(\Omega_i) \frac{\mathcal{T}_{ss,2}(\Omega_i) \delta(\theta_1 = \theta_i) \delta(\varphi_1 = \varphi_i)}{\cos(\theta_i) \sin(\theta_i)} r_{t,1}^{(1)}(\Omega_1 \rightarrow \Omega_2) \\ &\quad \frac{\tau_{oo,2}(\Omega_e) \delta(\theta_2 = \theta_e) \delta(\varphi_2 = \varphi_e)}{\cos(\theta_e) \sin(\theta_e)} \cos(\theta_i) \cos(\theta_1) \cos(\theta_2) d\Omega_i d\Omega_1 d\Omega_2, \\ &= \int_{\Pi} L_i(\Omega_i) \tau_{ss,2}(\Omega_i) r_{t,1}^{(1)}(\Omega_i \rightarrow \Omega_e) \tau_{oo,2}(\Omega_e) \cos(\theta_i) d\Omega_i, \\ &= \int_{-1}^{z_0} \int_{\Pi} L_i(\Omega_i) \exp[k(\Omega_i)z] \frac{w(\Omega_i, \Omega_e)}{\pi} \exp[K(\Omega_e)z] \cos(\theta_i) d\Omega_i dz. \end{aligned}$$

Now, for discrete leaves, and according to Eq. (17), the correlation between flux paths is taken into account as follows:

$$\mathcal{R}_{t,1} \mathcal{T}_{ss,2}[L_i](\Omega_e) = \int_{-1}^{z_0} \int_{\Pi} L_i(\Omega_i) \frac{w(\Omega_i, \Omega_e)}{\pi} \exp[(k(\Omega_i) + K(\Omega_e))z] C_{HS}(\Omega_i, \Omega_e, z) \cos(\theta_i) d\Omega_i dz.$$

Similarly, following the flux paths (Fig. 4), we obtain in the turbid case:

$$\begin{aligned} \mathcal{R}_{t,1} \mathcal{T}_{sd,2}[L_i](\Omega_e) &= \int_{-1}^{z_0} \int_{\Pi} \int_{\Pi} \underbrace{L_i(\Omega_i)}_{\text{Input}} \underbrace{\exp[k(\Omega_i)z]}_{N_1 \rightarrow M} \underbrace{\frac{w(\Omega_i, \Omega_e)}{\pi}}_M \underbrace{\exp[K(\Omega_e)(z-z_0)]}_{M \rightarrow P_2} \\ &\quad \underbrace{t_{d,2}(\Omega_0 \rightarrow \Omega_e)}_{P_2 \rightarrow T_1} \cos(\theta_i) \cos(\theta_0) d\Omega_i d\Omega_0 dz. \end{aligned} \quad (40)$$

In the discrete case, Eq. (40) becomes:

$$\begin{aligned} \mathcal{R}_{t,1} \mathcal{T}_{sd,2}[L_i](\Omega_e) &= \int_{-1}^{z_0} \int_{\Pi} \int_{\Pi} L_i(\Omega_i) \exp[k(\Omega_i)z] \frac{w(\Omega_i, \Omega_e)}{\pi} \\ &\quad \underbrace{\exp[K(\Omega_e)(z-z_0)] C_{HS}(\Omega_i, \Omega_e, z-z_0)}_{M \rightarrow P_2} \\ &\quad \underbrace{t_{d,2,HS}(\Omega_i, z, \Omega_0 \rightarrow \Omega_e)}_{P_2 \rightarrow T_1} \cos(\theta_i) \cos(\theta_0) d\Omega_i d\Omega_0 dz, \end{aligned} \quad (41)$$

By the same way, one has:

$$\begin{aligned} \mathcal{R}_{1,2} \mathcal{T}_{s,2}[L_i](\Omega_e) &= \int_{-1}^{z_0} \int_{\Pi} \int_{\Pi} L_i(\Omega_i) \exp[k(\Omega_i)z] \frac{w(\Omega_i, \Omega_e)}{\pi} \exp[K(\Omega_e)(z-z_0)] \\ &\quad C_{HS}(\Omega_i, \Omega_e, z-z_0) \underbrace{r_{b,2,HS}(\Omega_i, z, \Omega_0 \rightarrow \Omega_e)}_{P_2 \rightarrow R_3} \cos(\theta_i) \cos(\theta_0) d\Omega_i d\Omega_0 dz. \end{aligned} \quad (42)$$

3.4. AddingSD algorithm

As we have seen, the implementation in the discrete case should be harder than the turbid case and need the specification of many discretization details.

First, recall the computation of the first order hot spot effect. In the SAILH code implemented by Verhoef, a method to approximate the

first order reflectance ($r^{(1)}(\Omega_i \rightarrow \Omega_e)$) when the first order hot spot effect is taken into account is proposed. One has

$$r^{(1)}(\Omega_i \rightarrow \Omega_e) = \frac{w(\Omega_i, \Omega_e)}{\pi} \int_{-1}^0 \exp[(k(\Omega_i) + K(\Omega_e))z] C_{HS}(\Omega_i, \Omega_e, z) dz.$$

The interval $[-1, 0]$ is divided into $N_I=20$ subintervals $[a_{j+1}, a_j]$, $j \in \{0, \dots, N_I-1\}$, such that $a_0 = 0 > a_2 > \dots > a_{N_I} = -1$. $r^{(1)}$ is then written as follows:

$$r^{(1)}(\Omega_i \rightarrow \Omega_e) = \sum_{j=0}^{N_I-1} \underbrace{\frac{w(\Omega_i, \Omega_e)}{\pi} \int_{a_{j+1}}^{a_j} \exp[(k(\Omega_i) + K(\Omega_e))z] C_{HS}(\Omega_i, \Omega_e, z) dz}_{\text{hot}_j} \quad (43)$$

hot_j is then approximated for $j \in \{1, \dots, N_I-1\}$. For more information about the endpoint chosen and the integral approximation, view the SAILH code.

Now, the bidirectional reflectance corresponding to $\mathcal{R}_{t,1} \mathcal{T}_{ss,2}$ called $r_{t,1} t_{ss,2}$ is:

$$r_{t,1} t_{ss,2}(\Omega_i \rightarrow \Omega_e) = \frac{w(\Omega_i, \Omega_e)}{\pi} \int_{-1}^0 \exp[(k(\Omega_i) + K(\Omega_e))z] C_{HS}(\Omega_i, \Omega_e, z) dz.$$

So to derive this term, we perform the same discretization as for $r^{(1)}$ in Eq. (43) but the following modification. Let $k_0 \in \{0, \dots, N_I-1\}$, such that $a_{k_0+1} < z_0 \leq a_{k_0}$. a_{k_0} is then changed as follows: $a_{k_0} = z_0$, therefore the integral estimation is done over the points $(a_j)_{j \in \{k_0, \dots, N_I\}}$:

$$r_{t,1} t_{ss,2}(\Omega_i \rightarrow \Omega_e) = \sum_{j=k_0}^{N_I-1} \frac{w(\Omega_i, \Omega_e)}{\pi} \int_{a_{j+1}}^{a_j} \exp[(k(\Omega_i) + K(\Omega_e))z] C_{HS}(\Omega_i, \Omega_e, z) dz. \quad (44)$$

The bidirectional reflectance corresponding to $\mathcal{R}_{t,1} \mathcal{T}_{sd,2}$, called $r_{t,1} t_{sd,2}$ is:

$$r_{t,1} t_{sd,2}(\Omega_i \rightarrow \Omega_e) = \int_{-1}^0 \int_{\Pi} \exp[k(\Omega_i)z] \frac{w(\Omega_i, \Omega_o)}{\pi} \exp[K(\Omega_o)(z-z_0)] C_{HS}(\Omega_i, \Omega_o, z-z_0) t_{d,2,HS}(\Omega_i, z, \Omega_o \rightarrow \Omega_e) \cos(\theta_o) d\Omega_o dz.$$

By performing the same discretization as for $r_{t,1} t_{ss,2}$ Eq. (44), one obtains:

$$r_{t,1} t_{sd,2}(\Omega_i \rightarrow \Omega_e) = \sum_{j=k_0}^{N_I-1} \int_{\Pi} \int_{a_{j+1}}^{a_j} \exp[k(\Omega_i)z] \frac{w(\Omega_i, \Omega_o)}{\pi} \exp[K(\Omega_o)(z-z_0)] C_{HS}(\Omega_i, \Omega_o, z-z_0) t_{d,2,HS}(\Omega_i, z, \Omega_o \rightarrow \Omega_e) \cos(\theta_o) dz d\Omega_o. \quad (45)$$

Now, over each interval $[a_{j+1}, a_j]$, $t_{d,2,HS}(\Omega_i, z, \Omega_o \rightarrow \Omega_e)$ is assumed constant and it will be called $t_{d,2,HS,j}(\Omega_i, \Omega_o \rightarrow \Omega_e)$ and approximated by:

$$t_{d,2,HS,j}(\Omega_i, \Omega_o \rightarrow \Omega_e) \approx t_{d,2,HS} \left(\Omega_i, \frac{a_{j+1} + a_j}{2}, \Omega_o \rightarrow \Omega_e \right).$$

Recall that $t_{d,2,HS}$ is the diffuse bidirectional transmittance of the layer 2 derived using the 'effective' LAI_{HS} rather than LAI. The estimation of LAI_{HS} is performed using Eq. (24) and (45) becomes:

$$\begin{aligned} r_{t,1} t_{sd,2}(\Omega_i \rightarrow \Omega_e) &= \sum_{j=k_0}^{N_I-1} \int_{\Pi} \underbrace{\frac{w(\Omega_i, \Omega_o)}{\pi} \int_{a_{j+1}}^{a_j} \exp[k(\Omega_i)z] \exp[K(\Omega_o)(z-z_0)] C_{HS}(\Omega_i, \Omega_o, z-z_0) dz}_{\text{hot}_j(\Omega_i \rightarrow \Omega_o)} \\ &\quad t_{d,2,HS,j}(\Omega_i, \Omega_o \rightarrow \Omega_e) \cos(\theta_o) d\Omega_o, \\ &= \sum_{j=k_0}^{N_I-1} \int_{\Pi} \underbrace{\text{hot}_j(\Omega_i \rightarrow \Omega_o) t_{d,2,HS,j}(\Omega_i, \Omega_o \rightarrow \Omega_e) \cos(\theta_o) d\Omega_o}_{r_{t,1} t_{sd,2}(j, \Omega_i \rightarrow \Omega_e)}. \end{aligned} \quad (46)$$

Let $[R_{t,1} T_{sd,2}]_j$ and Hot_j be the discrete operators corresponding to the bidirectional terms $r_{t,1} t_{sd,2}(j, \Omega_i \rightarrow \Omega_e)$ and hot_j . Let $T_{d,2,HS,j,k}$ the

discrete operator corresponding to $t_{d,2,HS,j}$ for a value of the angle Ω_i equal $\Omega_{i,k}$. So, inspiring from the turbid case matrix product, it is easy to show that:

$$[R_{t,1} T_{sd,2}]_j(k, :) = \text{Hot}_j(k, :) T_{d,2,HS,j,k}, \quad (47)$$

with $[R_{t,1} T_{sd,2}]_j(k, :)$ (respectively $\text{Hot}_j(k, :)$) the matrix $[R_{t,1} T_{sd,2}]_j$ (respectively Hot_j) k th line (i.e. fixed value of Ω_i).

Let $R_{t,1} T_{sd,2}$ be the discrete operator corresponding to the bidirectional term $r_{t,1} t_{sd,2}(\Omega_i \rightarrow \Omega_e)$, then it can be written as follows:

$$R_{t,1} T_{sd,2} = \sum_{j=0}^{N_I-1} [R_{t,1} T_{sd,2}]_j. \quad (48)$$

By analogy with $T_{d,2,HS,j,k}$ in the discretization of $\mathcal{R}_{t,1} \mathcal{T}_{sd,2}$, one can define the discrete operator $R_{d,2,HS,j,k}$. Then, the discrete operator $R_{1,2} \mathcal{T}_{s,2}$ corresponding to $\mathcal{R}_{1,2} \mathcal{T}_{s,2}$ can be derived as $R_{t,1} T_{sd,2}$ by only replacing $T_{d,HS,j,k}$ by $R_{d,2,HS,j,k}$.

In summary, for a vegetation layer, the reflectance is computed dividing it into N_{HS} thin sublayers (LAI value equal L_{HS}), and iteratively adding a new sublayer to the current 'stack' of sublayers (from 1 to N_{HS}).

4. Method validation

The AddingS and AddingSD simulations are given for discrete operators by Eqs. (33) and (34) with a sample step equals to $\frac{1}{20} \pi$ for the zenithal angle and a sample step equals to $\frac{1}{10} \pi$ for the azimuthal angle. This discretization will be called (20,10). As it will be shown later, it is a compromise between computational considerations (memory and running time) and results accuracy. The leaf angle distribution is assumed ellipsoidal, parametrized by the mean leaf inclination angle, noted ALA, that varies between 0 and 90°. Small ALA values correspond to planophile vegetation and high ALA values to erectophile vegetation (Campbell, 1990). The elementary sublayer L_{\min} is chosen equal to 10^{-3} (enough to conserve energy, cf. Section 4.1). Finally, in the discrete case, when the multi hot spot is considered in the AddingSD model $L_{HS} = 3 \times 10^{-2}$.

In this section, first physical laws are checked. Secondly, a comparison between AddingS/AddingSD and SAIL/SAILH is given. Finally, validation tests based on the RAMI database are shown.

4.1. Physical laws

Among the physical laws that should be checked by a radiative transfer model, there are:

- i. Symmetry (reciprocity principle): the source and the observation positions are interchangeable;
- ii. Energy conservation: the quantity of radiation scattered by a medium is lower than the received one, the equality occurs where the medium does not absorb energy.

The symmetry induces that the positions of the source and the observation can be interchanged without changing the bidirectional reflectance. For an elementary sublayer, the bidirectional reflectance and transmittance are symmetric (Verhoef, 1985, 1998). For two successive vegetation layers 1 and 2, without making distinction both between the upward and the downward transmittances and between the top and the bottom reflectances, the total reflectance ($\mathcal{R}^{1,2}$) of the two layers is given by:

$$\mathcal{R}_t^{1,2} = \mathcal{R}_2 + \mathcal{T}_2 \circ (I - \mathcal{R}_1 \circ \mathcal{R}_2)^{-1} \circ \mathcal{R}_1 \circ \mathcal{T}_2,$$

where the subscript in the operators indicates the layer number. As the operators '+', '-', 'o' and '(.)⁻¹' preserve the symmetry. Therefore,

the bidirectional reflectance of the concatenation of the two layers is also symmetric.

For discrete operators, by accumulation of computation errors, the symmetry property of AddingS and AddingSD can be slightly violated,

the error can reach 0.4% for LAI=3. Hence, to preserve it, after each iteration the reflectance and transmittance matrices are symmetrized.

We will now focus on the energy conservation. For an elementary layer, it induces that for each source direction the sum of the

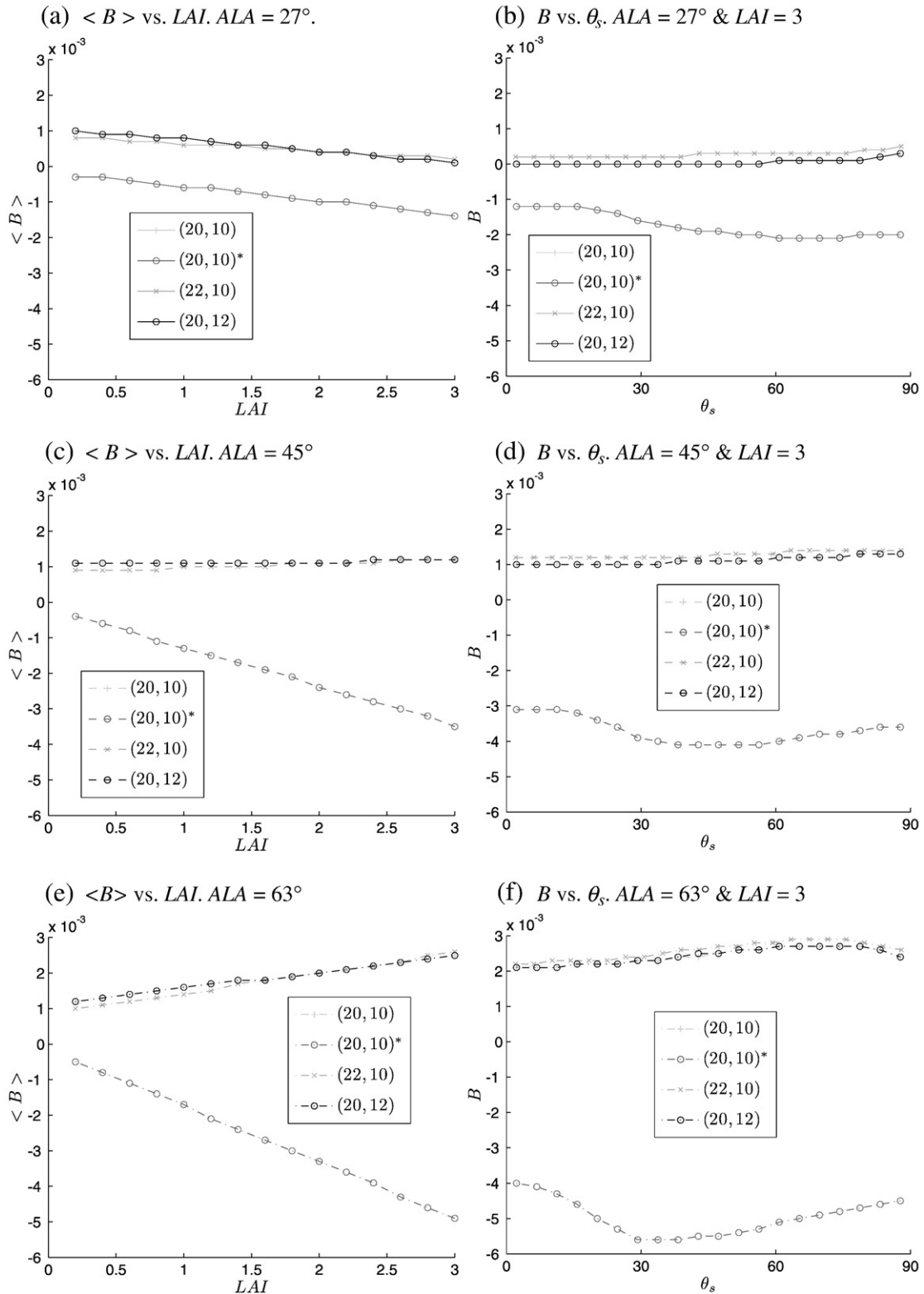


Fig. 8. Vegetation layer energy conservation in the turbid purist corner case: $\rho=0.5$ and $\tau=0.5$). In captions, the couple of values (x,y) corresponds to the zenithal (in $[0,\pi/2]$) and the azimuthal (in $[0,\pi]$) angle numbers of samples. (20,10)* is the only discretization such that the zenithal angle is not sampled regularly, the samples are: (5°, 15°, 25°, 35°, 45°, 55°, 64°, 68°, 72°, 75°, 77°, 79°, 81°, 83°, 85°, 86°, 87°, 88°, 88.5°, 89°).

directional hemispherical reflectance and the directional hemispherical diffuse transmittance is equal to the albedo ($\rho + \tau$) of the leaf multiplied by the intercepted flux:

$$\forall \Omega_s, \int_{\Pi} r_t(\Omega_s \rightarrow \Omega_o) \cos(\theta_o) d\Omega_o + \int_{\Pi} t_{d,d}(\Omega_s \rightarrow \Omega_o) \cos(\theta_o) d\Omega_o = k(\Omega_s)(\rho + \tau).$$

For an elementary layer, $r_t(\Omega_s \rightarrow \Omega_o) = \frac{1}{\pi} w(\Omega_s, \Omega_o)$ and $t_{d,d}(\Omega_s \rightarrow \Omega_o) = w_d(\Omega_s, \Omega_o)$ (w is divided by π because it corresponds to E_o which is equal to πL_o). Now, as shown in (Verhoef, 1998):

$$\frac{1}{\pi} \left[\int_{\Pi} w(\Omega_s, \Omega_o) \cos(\theta_o) d\Omega_o + \int_{\Pi} w_d(\Omega_s, \Omega_o) \cos(\theta_o) d\Omega_o \right] = k(\Omega_s)(\rho + \tau).$$

Receiving a direct source flux from a direction Ω_s , the total radiative budget ($B(\Omega_s)$) for one layer is given by the difference between the incident flux and the sum of the directional hemispherical reflectance and the total directional hemispherical transmittance:

$$B(\Omega_s) = 1 - \left[\int_{\Pi} \rho_t(\Omega_s \rightarrow \Omega_o) \cos(\theta_o) d\Omega_o + \int_{\Pi} (t_{d,d} + t_{d,s})(\Omega_s \rightarrow \Omega_o) \cos(\theta_o) d\Omega_o \right],$$

where

$$\int_{\Pi} t_{d,s}(\Omega_s \rightarrow \Omega_o) \cos(\theta_o) d\Omega_o = \tau_{ss}(\Omega_s) = \exp(-k(\Omega_s)).$$

For a thin layer, one has:

$$\int_{\Pi} t_{d,s}(\Omega_s \rightarrow \Omega_o) \cos(\theta_o) d\Omega_o \approx 1 - k(\Omega_s),$$

then

$$B(\Omega_s) = k(\Omega_s)(1 - \rho - \tau) \geq 0.$$

The equality is reached when $\rho + \tau = 1$ (purist corner case, pure scatterers, Pinty et al. (2004)), that corresponds to the fact that the leaves do not absorb any energy. For such leaves and for a system composed of a concatenation of thin sublayers, the radiative budget of the layer is hence equal to zero. Since the Adding method (on which based the AddingS model) as well as the generalized Adding method to the discrete case (that as led to the AddingSD model) represent all the interactions between the sublayers, the radiative budget of the global layer should also be equal to zero. In the following, to verify that our approach conserves the energy, we propose to check the value of B which should be close to zero. Practically, for visual comparison between simulations, the mean of $|B|$ values (noted $\langle |B| \rangle$) is convenient:

$$\langle |B| \rangle = \frac{1}{\pi} \int_{\Pi} |B(\Omega_s)| \cos(\theta_s) d\Omega_s.$$

In the turbid case, when using the AddingS model, the sign of B is constant (positive or negative), $\forall \Omega_s$. Therefore:

$$\langle B \rangle = \langle |B| \rangle \times \text{sign}(B).$$

And we chose finally to represent $\langle B \rangle$, since it can be viewed as the radiative budget of incident flux that is isotropically distributed over the hemisphere.

Table 1

Elementary operator derivation running time (in seconds) comparison between (20,10), (22,10) and (20,12)

| Discretization | (20,10) | (22,10) | (20,12) |
|------------------|---------|---------|---------|
| Running time (s) | 24.49 | 32.56 | 35.49 |

MATLAB code and PC P. 4, DELL OPT. GX 620, RAM 1 G.

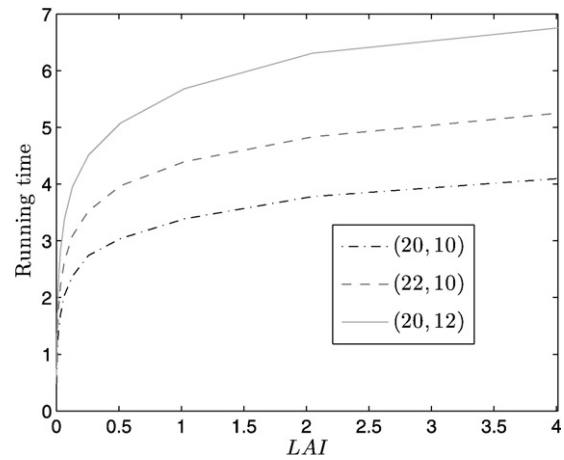


Fig. 9. Adding process running time (in seconds) comparison between (20,10), (22,10) and (20,12). MATLAB code and PC P.4, DELL OPT. GX 620, RAM 1 G.

Fig. 8 shows some energy conservation tests of the AddingS model varying LAI, ALA and θ_s for different kinds of discretization: (20,10), (20,10)*, (22,10) and (20,12). (20,10)* is a non-regular discretization corresponding to more samples for the higher values of zenithal angle

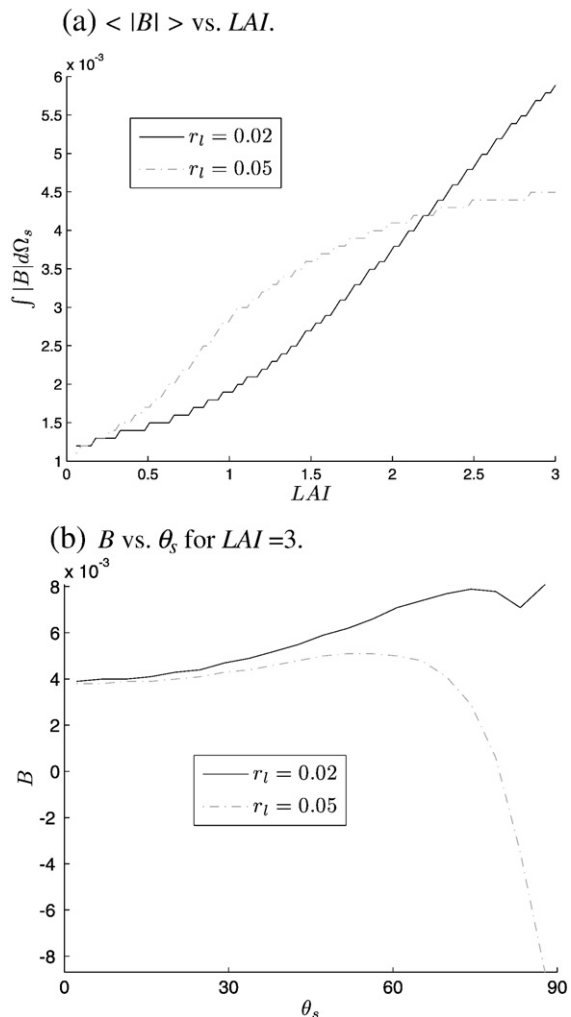


Fig. 10. Vegetation layer energy conservation in the discrete purist corner case: $\rho = 0.5$ and $\tau = 0.5$, for two values of hot spot parameter $r_l = 2\%$ and $r_l = 5\%$. ALA = 63° . The used discretization is (20,10).

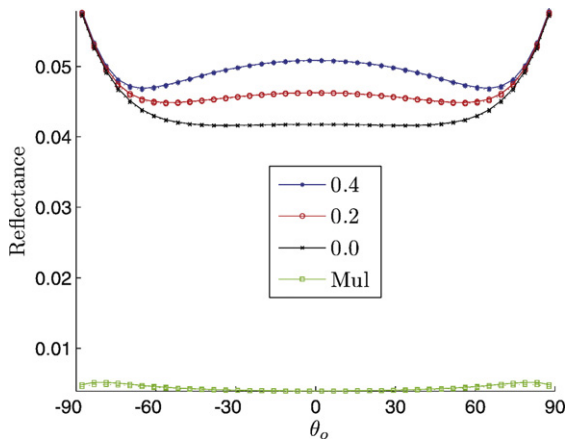


Fig. 11. BRDF measurements: turbid vegetation layer and Lambertian soil. LAI=3, ALA=45°, $\theta_s=30^\circ$, $\varphi_o=90^\circ$ and $(\rho, \tau)=(0.1,0.09)$. The solid and dotted line corresponds respectively to AddingS and SAIL results. The legend numerical values correspond to the used soil reflectance and 'Mul' refers to the layer multiple scattering contribution to the reflectance.

(input/output). First, we note that the error is always lower than 0.6% which means that the model conserves the energy. Besides, a phenomenon of error accumulation due to the discretization appears: the error increases with LAI (in particular on Fig. 8c,e). Note that $\langle B \rangle$

increases or decreases quasi-linearly. The three regular discretization give close results. (20,10), (20,12) give very close results, illustrating that the BRDF does not vary much versus the azimuthal angle. Mainly for low values of LAI (lower than 2), the discretization (22,10) gives more accurate results (than the two other regular discretizations): by increasing the number of samples over the zenithal angle, the performance of the model can be improved. Comparing the regular discretizations to the non-regular one, we see that the last one presents lower performance. Indeed, in the integrals the $\{r,t\}(\Omega_i \rightarrow \Omega_e)$ terms are weighted by $\cos(\theta_e)\sin(\theta_e)d\theta_e d\varphi_e$, that is (for $\theta_e > \pi/4$) as lower as the zenithal angle is high. Thus, a finer discretization for the higher values of the zenithal angle presents no interest in our case, which is clear on Fig. 8b,d,f: the error increases for $\theta_s > 30^\circ$ due to the decrease of the sample number from mid-values of zenithal angle. For the other discretization schemes, the error is about constant which confirms the interest of regular discretization for this study.

Still to test the energy conservation of our model, the directional hemispherical reflectance of a 'white' soil (reflectance equals 1) is derived using our model, the reflectance is estimated with an error of about $10^{-5}\%$.

Table 1 shows a comparison between the running times obtained for the computation of the elementary thin layer (L_{\min}) operators using the three discretizations: (20,10), (22,10) and (20,12). The running time increases by of about 33% (respectively 45%) when the zenithal angle (respectively the azimuthal angle) discretization is increased by only 2 samples (corresponding to an increase of the

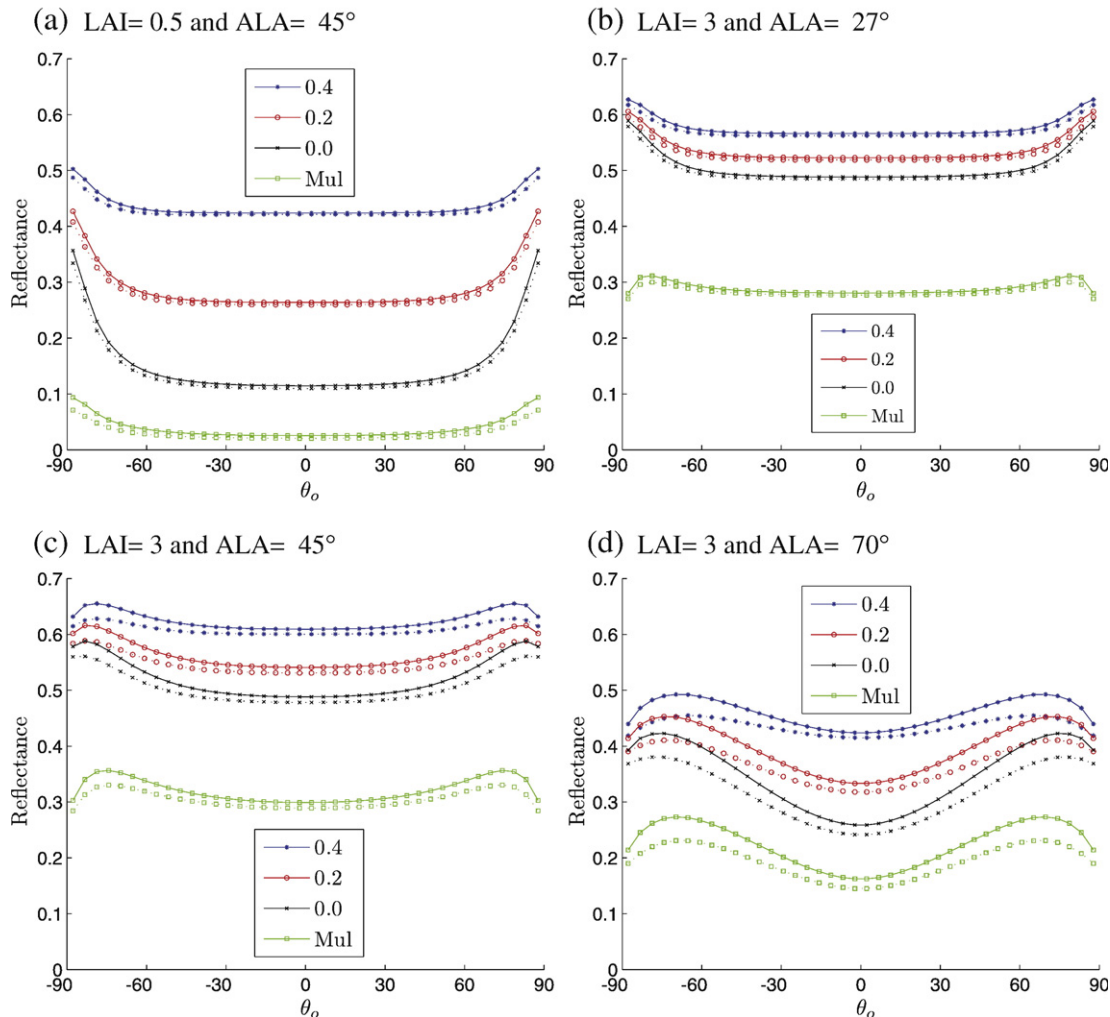


Fig. 12. BRDF measurements: turbid vegetation layer and Lambertian soil. $\theta_s=30^\circ$, $\varphi_o=90^\circ$ and $(\rho, \tau)=(0.47,0.49)$. The solid and dotted line correspond respectively to AddingS and SAIL results. The legend numerical values correspond to the used soil reflectance and 'Mul' refers to the layer multiple scattering contribution to the reflectance.

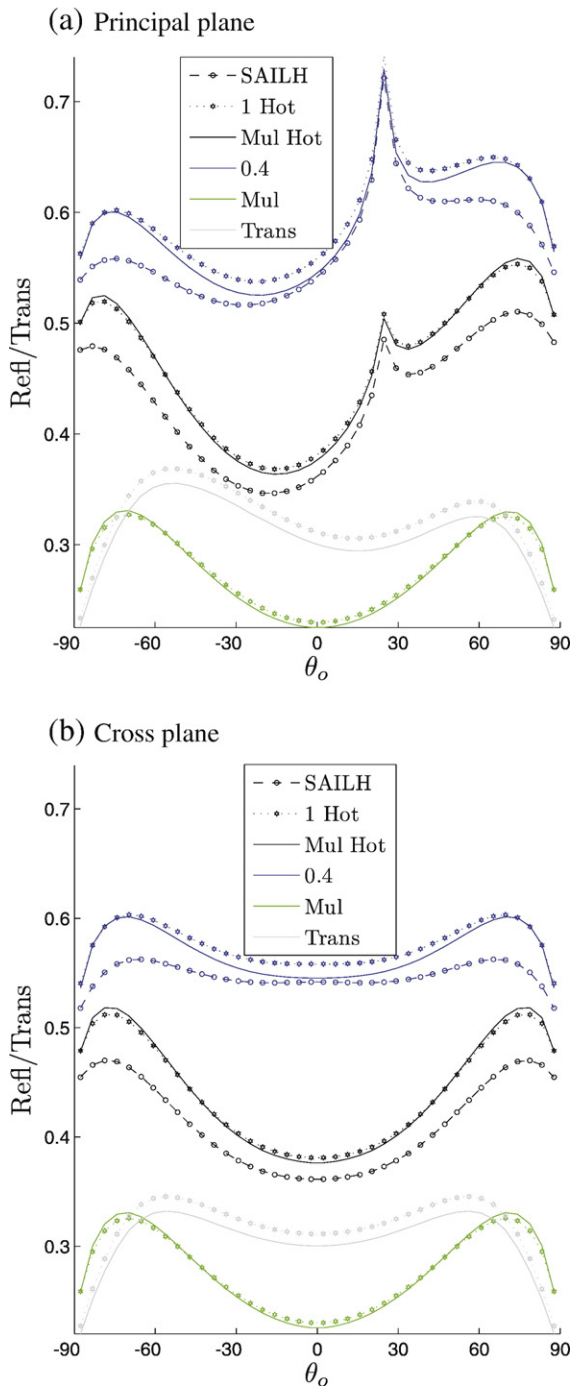


Fig. 13. Bidirectional reflectance and transmittance of canopy formed by a vegetation layer with LAI=3 covering the soil, ALA=63°, $\theta_s=25^\circ$, $(\rho, \tau)=(0.5,0.5)$ and $d_l=0.1$. The black curves present the layer BRDF. In the legend ‘1 Hot’, ‘Mul Hot’ means respectively the first order and the multi hot spot effect, ‘0.4’ is the used soil reflectance to compute top of canopy BRDF and ‘Mul’ means the layer multiple scattering contribution to the reflectance.

sample number of about 10%, respectively 20%). Fig. 9 shows a comparison between the running times obtained for the Adding process (concatenation of layers) using the same three discretizations. Once again, the running time increase is not linear and depends on LAI. For example for LAI=4, the running time increase is about 28% passing from (20,10) to (22,10) and about 65% from (20,10) to (20,12). For values of LAI lower than 3, we consider as sufficiently accurate the regular discretization (20,10).

Fig. 10 shows the variation of the energy balance of the AddingSD model in the purist corner case (a) versus LAI and (b) versus the source

zenithal angle θ_s for two values of hot spot parameter $r_l=0.02$ and $r_l=0.05$. Note that, due to the complexity of the discrete case, varying versus Ω_s , B can change sign, then we use $\langle |B| \rangle$ rather than $\langle B \rangle$, however, the difference between the two measure is too small. The error is always lower than 0.8%, so we conclude, like in the turbid case, that the method conserves the energy. We also note that like previously, the error increases with LAI. However, conversely to the turbid case, Fig. 10b shows that the error varies with the zenithal angle, that can be explained by the complexity of the multi hot spot model and the number of approximations used to compute integrals.

As shown in this section, both from theoretical study and simulations, our model verifies the symmetry property and the energy conservation. In the following section, a comparison with other models and a discussion are presented.

4.2. Our approach versus SAIL

Here, the simulation results given by the discrete AddingS and AddingSD models are assumed ‘credible’. We propose then a comparison of the canopy reflectance and transmittance simulations between SAIL/SAILH and AddingS/AddingSD.

Fig. 11 shows BRDF simulations, in the red wavelength domain, of a canopy composed of one vegetation layer covering the soil. As leaf scattering is low, the multiple scattering terms are negligible compared to the first order ones, inducing close SAIL and AddingS

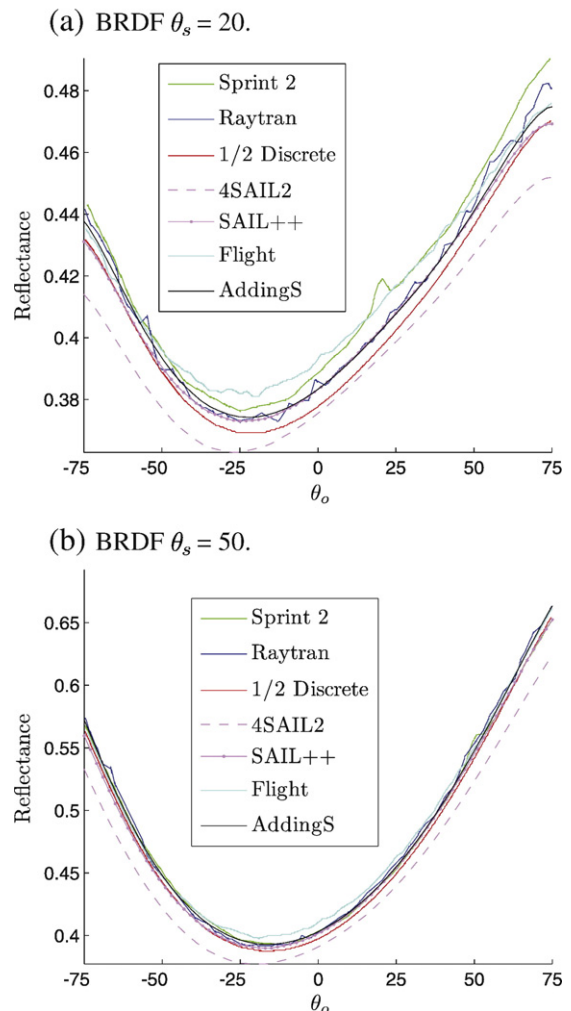


Fig. 14. Canopy BRDF simulation for turbid medium, principal plane. The vegetation features are LAI=3, $h=2$, uniform leaf distribution, $\rho=0.4957$ and $\tau=0.4409$. The soil is assumed Lambertian with reflectance equal to 0.159.

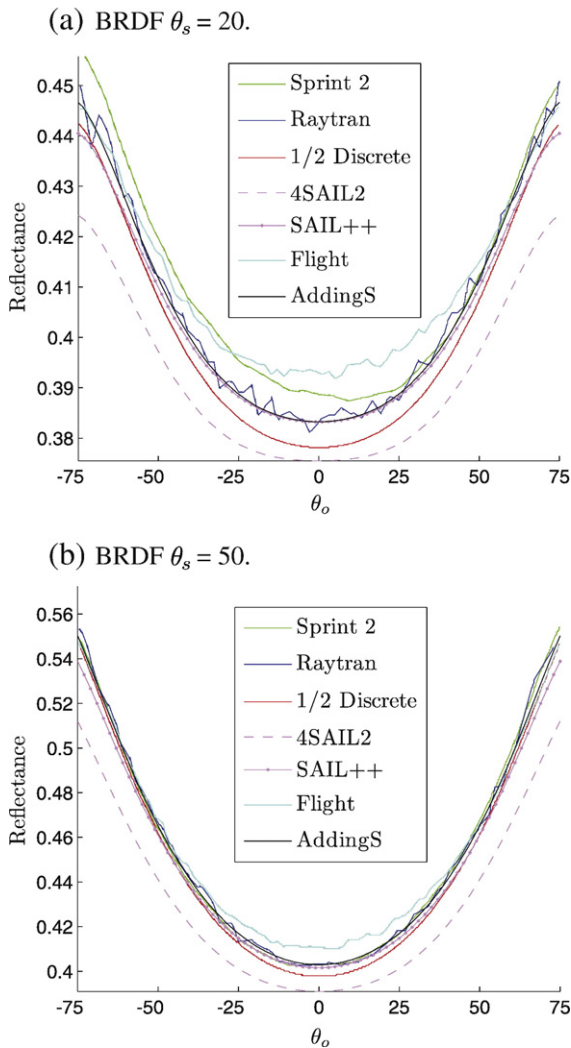


Fig. 15. Canopy BRDF simulation for turbid medium, cross plane. The vegetation features are LAI=3, $h=2$, uniform leaf distribution, $\rho=0.4957$ and $\tau=0.4409$. The soil is assumed Lambertian with reflectance equal to 0.159.

results. Note also that the BRDF increases with the soil reflectance. Fig. 12 shows different cases of comparison between the BRDF for one vegetation layer covering the soil in the Near Infrared domain. For low LAI values (Fig. 12.a), both models give close results. Indeed, in this case the reflectance essentially depends on the first order scattering term: the diffuse fluxes are negligible compared to the direct flux. Moreover, as the soil is Lambertian, the property that the layer BRDF increases versus the zenithal angle (Kallel, 2007) is as less marked as soil reflectance decreases. For higher LAI values and considering vegetation from planophile to erectophile, the difference between the two model results is more and more visible (Fig. 12.b,c,d). Indeed, as the agreement between SAIL and AddingS occurs for constant reflectance (Kallel, 2007) and as the variations of the multiple scattering reflectance are more and more important for higher zenith angles, the difference between the two models becomes stronger. This is even more prominent for vertical vegetation: the leaf reflectance being maximal for horizontal direction and minimal for vertical direction, the assumption of isotropically flux distribution is obviously false. In Fig. 12, we note also that when the soil reflectance increases, both the canopy BRDF increases and its angular variation is smoothed (Lambertian soil effect).

Fig. 13 shows a comparison between SAILH (Verhoef, 1998), the AddingSD model with the first order (1 Hot) and the multi hot spot

effect (Mul Hot). Since the multi hot spot effect conserves the energy, it is not surprising that the Mul Hot related curves are lower than the 1 Hot ones. However, we note the closeness of the vegetation layer Mul Hot reflectance simulation and the 1 Hot one. Indeed, referring to the 1 Hot reflectance, there are two additive contradictory effects: first the multi hot spot effect increases the reflectance, second the decrease of the multiple scattering fluxes decreases the total reflectance. Moreover, to conserve the energy the layer diffuse transmittance is necessary lower than the first order one, which is confirmed by the simulation. Since the layer transmittance is taken into account in the whole canopy reflectance computation, then by adding a bright soil, the Mul Hot BRDF curve becomes lower than the 1 Hot one. Note that, the differences are stronger for low zenithal angles and the results are close for high zenithal angles.

In agreement with the theoretical development, presented simulations have shown that SAIL underestimates the bidirectional reflectances of a vegetation layer. Note that in Verhoef (2002), the previous underestimation does not occur when adding a bright soil layer; however, this may be due to an overestimation of diffuse transmittance by SAIL. In the discrete case, the multi hot spot effect taken into account by the model AddingSD allows the conservation of the energy by the decrease of the diffuse transmittance.

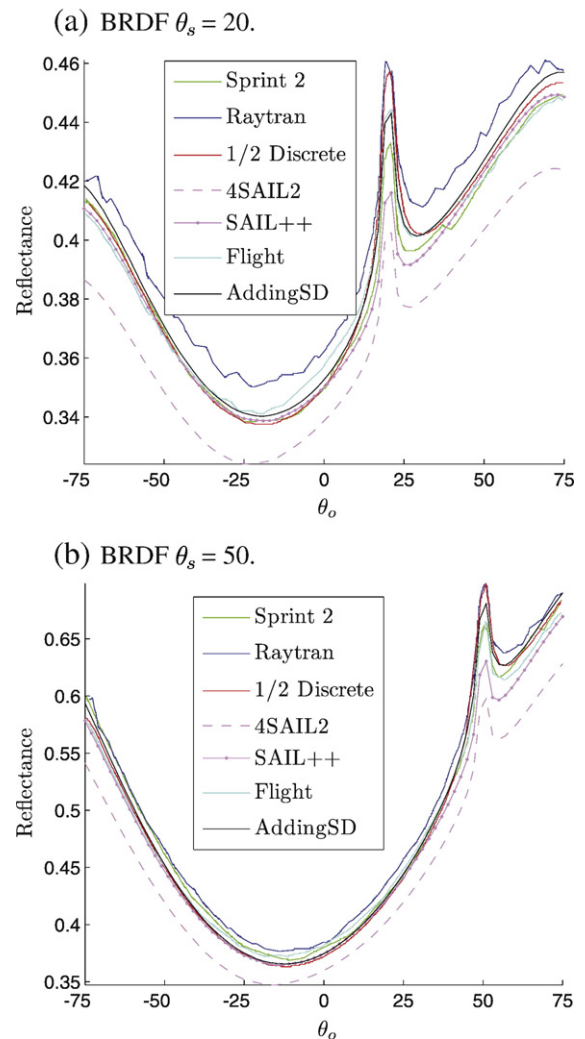


Fig. 16. Canopy BRDF simulations for discrete medium, principal plane. The vegetation features are LAI=3, $h=2$, leaf radius equal to 0.05, erectophile leaf distribution, $\rho=0.4957$ and $\tau=0.4409$. The soil is assumed Lambertian with reflectance equal to 0.159.

4.3. Method validation using the RAMI database

The RAdiation transfer Model Intercomparison (RAMI) database (Pinty et al., 2004) proposes some protocols to compare radiative transfer models applied to plant canopies covering soil surfaces. The object of RAMI is to point out enhancements which lead to some benefit for the remote sensing data interpretation and more generally lead to some benefit in terms of radiative transfer modeling and for the user communities.

The presented study only deals with homogenous vegetation layer for both turbid or discrete (finite size leaves) medium. Having tested numerous cases, we only present here the BRDF for the near-infrared domain, since the result for near-infrared domain are more contrasted than those obtained in the red domain. According to the RAMI second phase (Pinty et al., 2004), two kinds of radiative transfer model: 1-D models, namely 4SAIL2 (Verhoef & Bach, 2003, 2007), SAIL++ (Verhoef, 2002), 1/2 Discrete (Gobron et al., 1997), and 3-D models, namely Flight (North, 1996), DART (Gastellu-Etchegorry et al., 1996), Sprint-2 (Thompson & Goel, 1998), Raytran (Govaerts & Verstraete, 1998), RGM (Qin & Sig, 2000), Drat (Lewis, 1999), have been considered (for comparison with our approach). In the lack of ground truth data, the 3-D models are taken as references. According to the RAMI phase 2

simulation results “Flight, Raytran and Sprint-2 are the most credible models”. Recall that the proposed models (AddingS and AddingSD) are 1-D models. In this section, we will show that these 1-D models compete, in terms of result accuracy, with the ‘most credible’ 3-D models and are more credible than classical 1-D models, such as the 4SAIL2 or the 1/2 Discrete models. It will be also shown that SAIL++ gives results close to the AddingS and AddingSD ones. For legibility, only the ‘most credible’ 3-D models and among the 1-D models 4SAIL2, SAIL++, 1/2 Discrete and AddingS/AddingSD are shown. Note that, to conform with the RAMI simulations, the Bunnik (1978) leaf distribution was used for our simulations.

Figs. 14 and 15 show the BRDF simulations in the case of a turbid medium. Fig. 14a and b (respectively Fig. 15a and b) show simulations in the principal plane (respectively in the cross plane) differing by the source zenithal angle. For all simulations, the AddingS curve is intermediate between the 3-D model curves. As shown in the last Section 4.2, the 4SAIL2 model underestimates the bidirectional reflectance. Since the SAIL++ model overcomes the isotropy assumption, SAIL++ gives good results close to the AddingS ones even if they are sometimes slightly below the 3-D models. We also see that the 1/2 Discrete curve is always below the 3-D model curves. Finally, for near nadir observations, the Flight model curve is above the others.

Figs. 16 and 17 are the equivalent of Figs. 14 and 15 for a discrete medium. As previously, our model (here AddingSD) simulation is intermediate between the 3-D model simulations, which is not true for the other 1-D models. As seen previously, the 4SAIL2 model underestimates the BRDF. As the soil reflectance is small, the multi hot spot effect results are close to the first order ones and so AddingSD and SAIL++ give close results. Finally, we note that the Raytran simulations are always above the other 3-D simulations, in particular for near nadir observations.

In conclusion, based on 3-D simulations, assumed close to the ‘truth’, our model shows better performance than the other 1-D models.

5. Conclusion

In this paper, a coupling between SAIL and Adding was shown. First, a new mathematical formalism for the Adding method operators has been proposed. For a given layer, the operators are derived using the SAIL model formalism. Since the SAIL model gives accurate results for low LAI values (the diffuse fluxes are negligible for thin layers), the different operator parameters were derived for a thin layer. Then, the layers with high LAI values were decomposed into thin sublayers in which the operators are derived, and using the Adding principles, the global layer operators are computed; the proposed model is called AddingS. Such an approach allows to overcome the assumption of SAIL that diffuse fluxes are isotropically distributed. In the discrete case, we proposed an extension of the Kuusk model to our model; the extended model is called AddingSD, and we showed that the hot spot effect corresponds to a local reduction of the LAI. All scattering terms are hence estimated using the modified values of LAI, allowing energy conservation. Since, the proposed method takes into account the hot spot effect between diffuse fluxes, we call it ‘the multi hot spot effect’.

The validation was performed according to three kinds of tests. First, the model physical laws are presented: energy conservation and symmetry between source and observation. Secondly, we compare SAIL (or SAILH) and AddingS (or AddingSD either with only the first order hot spot effect, or modeling the multi hot spot effect): we showed that SAIL underestimates the reflectance whereas the first order hot spot overestimates it. Finally, based on the RAMI II database, it is shown that our models (AddingS and AddingSD) give results comparable to those obtained by 3-D radiative transfer models.

From computational point of view, AddingS and AddingSD take much longer running time than 4SAIL2 and SAIL++. Moreover, compared to the Adding version of (Cooper et al., 1982), our

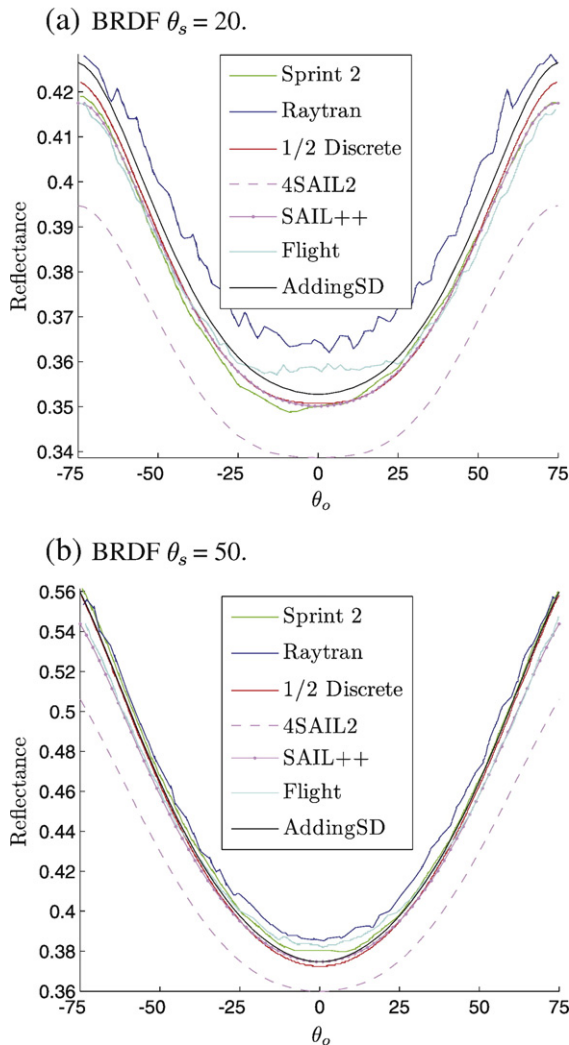


Fig. 17. Canopy BRDF simulations for discrete medium, cross plane. The vegetation features are LAI=3, $h=2$, leaf radius equal to 0.05, erectophile leaf distribution, $\rho=0.4957$ and $\tau=0.4409$. The soil is assumed Lambertian with reflectance equal to 0.159.

algorithms are more complex and 'longer'. Therefore, using simple approximations of the multiple scattering fluxes, SAIL gives good approximation of the BRDF mainly in the Visible/InfraRed domain excluding the NIR; making AddingS and AddingSD really interesting only in the NIR domain.

Although our approach claims to model many physical phenomena describing the interaction wave/canopy such as multiple scattering and multi hot spot effect, we emphasize that many assumptions are no other than an idealization of the actual canopy case: e.g., the leaves are Lambertian discs having the same radius. Future study will deal with such phenomena. Moreover, we would like to extend the model to the thermal domain.

Acknowledgments

This work was funded by the French national programme, INSU-PNTS. Particular thanks are to the French Space Agency, CNES and to Bretagne regional direction, for the scholarship support they provided for this study. The authors are also grateful to F. Baret and B. Coudert for the constructive discussions.

References

- Allen, W. A., Gayle, T. V., & Richardson, A. J. (1970). Plan canopy irradiance specified by the Duntley equations. *Journal of Optic Society of America*, 60(3), 372–376.
- Bunnik, N. (1978). The multispectral reflectance of shortwave radiation of agricultural crops in relation with their morphological and optical properties. *Tech. rep., Mededelingen Landbouwhogeschool, Wageningen, the Netherlands*.
- Campbell, G. S. (1990). Derivation of an angle density function for canopies with ellipsoidal leaf angle distribution. *Agricultural and Forest Meteorology*, 49, 173–176.
- Chandrasekhar, S. (1950). *Radiative Transfer*. New-York: Dover.
- Combal, B., Baret, F., Weiss, M., Trubuil, A., Macé, D., Pragnère, A., My-neni, R., Knyazikhin, Y., & Wang, L. (2002). Retrieval of canopy biophysical variables from bidirectional reflectance using prior information to solve the ill-posed inverse problem. *Remote Sensing of Environment*, 84, 1–15.
- Cooper, K., Smith, J. A., & Pitts, D. (1982). Reflectance of a vegetation canopy using the adding method. *Applied Optics*, 21(22), 4112–4118.
- Fanga, H., Lianga, S., & Kuusk, A. (2003). Retrieving leaf area index using a genetic algorithm with a canopy radiative transfer model. *Remote Sensing of Environment*, 85, 257–270.
- Gastellu-Etchegorry, J., Demarez, V., Pinel, V., & Zagolski, F. (1996). Modeling radiative transfer in heterogeneous 3-d vegetation canopies. *Remote Sensing of Environment*, 58, 131–156.
- Gobron, N., Pinty, B., Verstraete, M., & Govaerts, Y. (1997). A semidiscrete model for the scattering of light by vegetation. *Journal of Geophysical Research*, 102, 9431–9446.
- Govaerts, Y., & Verstraete, M. M. (1998). Raytran: A Monte Carlo ray tracing model to compute light scattering in three-dimensional heterogeneous media. *IEEE Transactions on Geoscience and Remote Sensing*, 36, 493–505.
- Hapke, B. (1981). Bidirectional reflectance spectroscopy. 1. Theory. *Journal of Geophysical Research*, 86, 3039–3054.
- Jacquemoud, S., & Baret, F. (1990). Prospect: A model of leaf optical properties spectra. *Remote Sensing of Environment*, 34(2), 75–91.
- Kallel, A. (2007). Inversion d'images satellites 'haute résolution' visible/infrarouge pour le suivi de la couverture végétale des sols en hiver par modélisation du transfert radiatif, fusion de données et classification. Ph.D. thesis, Orsay University.
- Kokhanovsky, A. (Ed.). (2007). *Light Scattering Reviews 2*. Springer.
- Kuusk, A. (1985). The hot spot effect of a uniform vegetative cover. *Sovietic Journal of Remote Sensing*, 3(4), 645–658.
- Kuusk, A. (1991a). Determination of vegetation canopy parameters from optical measurements. *Remote Sensing of Environment*, 37, 207–218.
- Kuusk, A. (1991b). The hot spot effect in plant canopy reflectance. In R. I. Myneni & J. Ross (Eds.), *Photon-vegetation interactions. Applications in optical remote sensing and plant ecology* (pp. 139–159). Berlin: Springer.
- Kuusk, A. (1994). Multispectral canopy reflectance model. *Remote Sensing of Environment*, 50, 75–82.
- Kuusk, A. (1995a). A fast, invertible canopy reflectance model. *Remote Sensing of Environment*, 51, 342–350.
- Kuusk, A. (1995b). Markov chain model of canopy reflectance. *Agriculture Forest Meteorology*, 76, 221–236.
- Lenoble, J. (1985). *Radiative transfer in scattering and absorbing atmospheres: Standard computational procedures*. Hampton, VA.
- Lewis, P. (1999). Three-dimensional plant modelling for remote sensing simulation studies using the botanical plant modelling system. *Agronomie-Agriculture and Environment*, 19, 185–210.
- North, P. (1996). Three-dimensional forest light interaction model using a Monte Carlo method. *IEEE Transactions on Geoscience and Remote Sensing*, 34, 946–956.
- Pinty, B., Widlowski, J., Taberner, M., Gobron, N., Verstraete, M., Disney, M., Gascon, F., Gastellu, J., Jiang, L., Kuusk, A., Lewis, P., Li, X., Ni-Meister, W., Nilson, T., North, P., Qin, W., Su, L., Tang, R., Thompson, R., Verhoef, W., Wang, H., Wang, J., Yan, G., & Zang, H. (2004). The RAdiation transfer Model Intercomparison (RAMI) exercise: Results from the second phase. *Journal of Geophysical Research*, 109.
- Qin, W., & Sig, A. (2000). 3-d scene modeling of semi-desert vegetation cover and its radiation regime. *Remote Sensing of Environment*, 74, 145–162.
- Smith, J. A., Ranson, K. J., Nguyen, D., Balick, L., Link, E., Fritschen, L., & Hutchison, B. (1981). Thermal vegetation canopy model studies. *Remote Sensing of Environment*, 11, 311–326.
- Suits, G. H. (1972). The calculation of the directional reflectance of a vegetative canopy. *Remote Sensing of Environment*, 2, 117–125.
- Thompson, R., & Goel, N. S. (1998). Two models for rapidly calculating bidirectional reflectance: Photon spread (ps) model and statistical photon spread (sps) model. *Remote Sensing Reviews*, 16, 157–207.
- Van de Hulst, H. C. (1981). *Light Scattering by Small Particles*. New York: Dover Publications, Inc.
- Verhoef, W. (1984). Light scattering by leaf layers with application to canopy reflectance modelling: The sail model. *Remote Sensing of Environment*, 16, 125–141.
- Verhoef, W. (1985). Earth observation modeling based on layer scattering matrices. *Remote Sensing of Environment*, 17, 165–178.
- Verhoef, W. (1998). Theory of radiative transfer models applied to optical remote sensing of vegetation canopies. Ph.D. thesis, Agricultural University, Wageningen, The Netherlands.
- Verhoef, W. (2002). Improved modelling of multiple scattering in leaf canopies: The model: Sail++. *Proceedings of the First Symposium on Recent Advances in Quantitative Remote Sensing* (pp. 11–20). Spain: Torrent.
- Verhoef, W., & Bach, H. (2003). Simulation of hyperspectral and directional radiance images using coupled biophysical and atmospheric radiative transfer models. *Remote Sensing of Environment*, 87, 23–41.
- Verhoef, W., & Bach, H. (2007). Coupled soil leaf canopy and atmosphere radiative transfer modeling to simulate hyperspectral multi-angular surface reflectance and TOA radiance data. *Remote Sensing of Environment*, 109(2), 166–182.
- Verstraete, M. M., Pinty, B., & Dickinson, R. E. (1990a). A physical model of the bidirectional reflectance of vegetation canopies, part 1: Theory. *Journal of Geophysical Research*, 95, 11755–11765.
- Verstraete, M. M., Pinty, B., & Dickinson, R. E. (1990b). A physical model of the bidirectional reflectance of vegetation canopies, part 2: Inversion and validation. *Journal of Geophysical Research*, 95, 11767–11775.